HHS Public Access

Author manuscript

Exp Eye Res. Author manuscript; available in PMC 2016 December 01.

Published in final edited form as:

Exp Eye Res. 2015 December ; 141: 139–153. doi:10.1016/j.exer.2015.06.001.

In vivo imaging methods to assess glaucomatous optic neuropathy

Brad Fortune

Discoveries in Sight Research Laboratories, Devers Eye Institute and Legacy Research Institute, Legacy Health, Portland, OR, USA

Abstract

The goal of this review is to summarize the most common imaging methods currently applied for in vivo assessment of ocular structure in animal models of experimental glaucoma with an emphasis on translational relevance to clinical studies of the human disease. The most common techniques in current use include optical coherence tomography and scanning laser ophthalmoscopy. In reviewing the application of these and other imaging modalities to study glaucomatous optic neuropathy, this article is organized into three major sections: 1) imaging the optic nerve head, 2) imaging the retinal nerve fiber layer and 3) imaging retinal ganglion cell soma and dendrites. The article concludes with a brief section on possible future directions.

Keywords

glaucoma; experimental models; optical coherence tomography; scanning laser ophthalmoscopy; scanning laser polarimetry; adaptive optics; optic nerve; retinal ganglion cells; retinal nerve fiber layer

Introduction

Glaucoma is the most common optic neuropathy and the second leading cause of blindness worldwide.(Quigley and Broman, 2006) Vision loss in glaucoma occurs primarily because retinal ganglion cells (RGCs) die and their axons degenerate, losing the capacity to convey visual information to the brain.(Quigley, 1999, 2011; Quigley et al., 1981; Weinreb and Khaw, 2004) The initiating injury to RGCs and their axons is thought to occur within the optic nerve head (ONH).(Anderson and Hendrickson, 1974; Emery et al., 1974; Howell et al., 2012; Nickells et al., 2012; Quigley, 1999; Quigley et al., 1981; Vrabec, 1976) Indeed, chronic progressive deformation of the ONH tissues (traditionally referred to as “cupping” and/or “excavation”) is considered the hallmark of glaucoma, a clinical sign used to

Correspondence: Brad Fortune, OD, PhD, Associate Scientist, Devers Eye Institute, 1225 NE Second Avenue, Portland, OR 97232, Phone: 503-413-1198, Fax: 503-413-5179, bfortune@deverseye.org.

Commercial Disclosures: Heidelberg Engineering, GmbH, Heidelberg, Germany (equipment support); Carl Zeiss Meditec, Inc. (equipment).

distinguish it from other optic neuropathies.(Danesh-Meyer et al., 2009; Quigley, 1993, 2011; Van Buskirk and Cioffi, 1992; Weinreb and Khaw, 2004) Thus clinical diagnosis and management of glaucoma depend not only on assessment of vision function, such as by measuring sensitivity across the visual field using automated perimetry, but also on assessment of structural integrity of the ONH and RGC axons within the retinal nerve fiber layer (RNFL).

Assessment of ONH and RNFL structural integrity can be achieved most easily by clinical examination using a direct ophthalmoscope, however, appreciation of finer detail is afforded by stereoscopic examination using binocular indirect ophthalmoscopy. Similarly, archival records of ONH and RNFL structure can be achieved in simplest form using a two-dimensional drawing or flash photograph, but simultaneous stereoscopic photographs offer superior capability for discerning changes in ONH surface topopgraphy due to their three-dimensionality.

More recent developments in ophthalmic imaging technology have enabled *quantification* of structural parameters, such as the width or volume of optic disc rim tissue, width and depth of the optic cup and cup-to-disc ratio, etc. One such technique known as confocal scanning laser tomography (CSLT) has become widely incorporated into both glaucoma research and clinical practice, and has even been used as an ancillary outcome measure for randomized clinical trials.(Alencar et al., 2008, 2005; Sharma et al., 2008; Wollstein et al., 2000; Zangwill et al., 2013; Zangwill et al., 2005) Optical coherence tomography (OCT) enables cross-sectional images of ONH and retinal tissue to be acquired in the living eye and thus quantification of individual retinal layer thicknesses, as well as three-dimensional (3D) visualization and quantification of deeper ONH structures such as the lamina cribrosa (LC). (Inoue et al., 2009; Kagemann et al., 2008; Srinivasan et al., 2008; Strouthidis et al., 2009; Wollstein et al., 2005a) Modern OCT systems provide axial resolution of a few micrometers and the addition of adaptive-optics techniques are able to improve lateral (transverse) resolution to the same level.(Hermann et al., 2004; Kocaoglu et al., 2011; Kocaoglu et al., 2014a; Kocaoglu et al., 2014b; Torti et al., 2009; Zawadzki et al., 2009; Zawadzki et al., 2005; Zhang et al., 2005) These most recent developments hold great promise for helping to elucidate directly from studies performed in clinical settings a more precise understanding of glaucoma risk, the susceptibility of individual eyes and even the sequence of events in glaucoma pathogenesis.

Yet experimental models of glaucoma remain important for these purposes, for testing hypothesis about pathogenesis and for pre-clinical trials of novel therapeutic interventions (reviewed elsewhere this issue and others, e.g., (Burgoyne et al., 2005; Goldblum and Mittag, 2002; Morrison et al., 2008; Pang and Clark, 2007)). Common outcome measures for experimental glaucoma (EG) models include histological counts of RGC soma and/or orbital optic nerve axons, which require euthanasia and are thus only available at a single time point. Outcome measures based on *in vivo* imaging techniques, such as those used in the clinical setting and mentioned above, enable longitudinal evaluation within animals. Benefits of longitudinal imaging include reduction of the number of animals required to adequately power a scientific study (instead of sacrificing a different set of animals at each time point) and mitigation against errors that can arise when inferences about longitudinal

time course and inter-relationships are drawn from cross-sectional data.(Naskar et al., 2002; Prilloff et al., 2010; Sabel et al., 1997; Thanos et al., 2002) Moreover, application of imaging techniques that can be used across the spectrum of laboratory and pre-clinical studies in animals as well as clinical research and patient management in human glaucoma enables similar outcome measures to be assessed in order to better compare the pathophysiological sequence of an experimental model with the human disease. Such approaches may facilitate future translation of novel interventions and to ensure relevance and/or refine any given EG model accordingly. This review article summarizes the most common imaging methods currently applied for *in vivo* assessment of ocular structure in EG models with an emphasis on translation to clinical studies of the human disease. It is organized into three main sections based on target structure: ONH, RNFL, RGC soma and dendrites. Generally, since most ophthalmic imaging modalities were originally developed for clinical use in human eyes and then later adapted for use in animals, the discussion of each modality and target structure begins with some relevant background on development and application to basic and clinical studies of human eyes, then continues with laboratory studies in animals. It is hoped that this organizational structure will help emphasize the bidirectional translational nature of imaging in glaucoma research.

1. Imaging the ONH

Essentially any imaging modality used in a clinical setting for imaging human eyes can also be applied for imaging the eyes of larger laboratory animals - such as monkeys - with only minor modifications of technique to maintain optimal alignment, focus and corneal hydration since the latter are generally imaged under anesthesia. It is more challenging to image eyes of smaller laboratory animals such as rats and mice, primarily due to their smaller pupil size, higher optical power and aberrations. Thus, fundus photography in rats and mice benefits greatly from specialized equipment arrangements and procedures in order to obtain higher quality fundus images.(Cohan et al., 2003; Hawes et al., 1999; Kocaoglu et al., 2007; Paques et al., 2007) High-resolution images of the mouse or rat fundus can also be obtained by confocal scanning laser ophthalmoscopy (CSLO).(Chauhan et al., 2002; Cordeiro et al., 2004; Paques et al., 2006; Seeliger et al., 2005) Advantages of CSLO for fundus imaging include improved image contrast due the confocal aperture and relative ease of imaging through the smaller pupil due to the narrow diameter of the scanning beam; disadvantages include greater expense of CSLO systems and lack of true color reflectance since the imaging source is monochromatic, though this aspect also contributes to greater image contrast and facilitates fluorescence applications.(Cordeiro et al., 2004; Paques et al., 2006; Seeliger et al., 2005)

CSLO has been used to image the LC *in vivo* and perform quantitative morphometry in healthy and glaucomatous human eyes, measurements that were previously approachable only by histology. One of the earliest of such studies demonstrated that elongation of LC pores is related to the severity of glaucomatous visual field damage.(Fontana et al., 1998) The addition of adaptive-optics (AO) to compensate for optical aberrations(Burns et al., 2007; Liang et al., 1997; Roorda et al., 2002) provides higher resolution in both transverse and axial dimensions for SLO imaging, which is particularly important for morphometric analysis of a complex three-dimensional structure such as the LC.(Akagi et al., 2012; Ivers

et al., 2011; Sredar et al., 2013; Vilupuru et al., 2007) Nevertheless, SLO imaging of the LC is ultimately limited to the visible portions of its anterior surface, which is masked across much of the ONH by major blood vessel branches and overlying rim tissue (consisting of axon bundles, astroglia and capillaries, all sources of scatter). Moreover, the LC of the rat ONH has only a few wispy vertical collagenous beams(Morrison et al., 1995) while the mouse ONH has none(May and Lutjen-Drecoll, 2002; Sun et al., 2009) and the major vessel branches also occupy a much greater proportion of the "optic disc" in rats and mice as compared with human and non-human primate (NHP) eyes.(Chauhan et al., 2002; Fortune et al., 2011; Guo et al., 2005; Srinivasan et al., 2006; Zhi et al., 2011; Zhi et al., 2012) Thus the applicability of two-dimensional *reflectance* imaging of the ONH in rat or mouse EG models is limited. However, Bosco and colleagues recently used *fluorescence* CSLO imaging *in vivo* to document early-stage ONH microgliosis in the DBA/2J mouse model of inherited glaucoma.(Bosco et al., 2015) Ho et al., have also used in vivo longitudinal CSLO imaging to document gliotic responses of astrocytes within the ONH after RGC injury.(Ho et al., 2009)

OCT imaging provides much higher axial resolution (~ two orders of magnitude better) than CSLO, which has proven important to 3D visualization of the human LC.(Inoue et al., 2009; Kagemann et al., 2008; Srinivasan et al., 2008) Use of the "enhanced depth imaging" (EDI) mode(Lee et al., 2012; Park et al., 2012a; Park et al., 2012b; Yang et al., 2012a) and related strategies(Kim et al., 2012) in order to mitigate the signal roll-off inherent to spectral domain OCT improves measurement reliability and has revealed focal LC structural alterations that relate to glaucomatous disease severity.(Faridi et al., 2014; Tatham et al., 2014; You et al., 2013) Similarly, postprocessing techniques can be applied to recover contrast lost to signal attenuation(Girard et al., 2015; Mari et al., 2013) and further improve OCT imaging of deep ONH structures. The increased penetration of longer wavelength OCT sources (e.g. center wavelength of 1050 nm), such as those typically used in swept-source OCT may also improve imaging of the LC, peripapillary sclera and deep ONH structures. (Srinivasan et al., 2008; Takayama et al., 2013a; Wang et al., 2013; Yoshikawa et al., 2014) Using polarization-sensitive swept-source OCT imaging at 1μm further enhances visualization of these strongly birefringent connective tissues.(Yamanari et al., 2009) However, one trade-off of the longer wavelength is a slight reduction of transverse resolution and the narrower frequency band available for most swept-source lasers results in reduced axial resolution (as compared with spectral domain OCT). These trade-offs can be overcome using adaptive optics, which enables 3D visualization *in vivo* of retinal and ONH anatomy at a cellular scale (Kocaoglu et al., 2011; Kocaoglu et al., 2014a; Kocaoglu et al., 2014b; Torti et al., 2009; Zawadzki et al., 2009) and reliable morphometry of LC microarchitecture in the living human eye.(Nadler et al., 2014a; Nadler et al., 2014b) Yet masking by the major vessel branches remains an important constraint on all OCT imaging of the LC.

Spectral domain OCT (SDOCT) has been used to reveal early-stage ONH changes *in vivo* in a unilateral, inducible model of EG in NHP based on chronic, mild-to-moderate elevation of intraocular pressure (IOP).(He et al., 2014; Strouthidis et al., 2011b; Yang et al., 2014; Yang et al., 2012a) Specifically, SDOCT studies have shown that LC changes such as an increase

in the depth of its anterior surface precede peripapillary RNFL thinning, another OCT-derived parameter now commonly used in clinical management of glaucoma.(He et al., 2014; Strouthidis et al., 2011b; Yang et al., 2014) Further evidence that ONH changes precede thinning of the peripapillary RNFL in this NHP EG model has been reported for studies that used CSLT for longitudinal assessment of ONH surface topography.(Fortune et al., 2012; Fortune et al., 2013b; He et al., 2014; Strouthidis et al., 2011b) Collectively, these studies demonstrate clearly that ONH changes occur at a very early stage in the NHP EG model, prior to loss of RNFL thickness measured adjacent to the ONH as is typically done clinically for glaucoma management. What remains to be determined is whether any or all of these early-stage ONH changes, such as changes in the depth of the anterior LC surface, alterations of LC microarchitecture, pore size and shape, or changes in ONH surface topography are specifically predictive of subsequent RGC injury and axon loss such that they should be considered clinical indicators for therapeutic intervention. In contrast, current evidence from the NHP EG model indicates that the first detectable loss of peripapillary RNFL thickness is already associated with 10–15% loss of axons from the orbital optic nerve,(Cull et al., 2012, 2014) suggesting that earlier indicators are needed for timely treatment intervention.

Another exciting question that remains to be answered is whether aspects of ONH structure measured *in vivo* by OCT or other techniques will serve as specific predictors of glaucoma risk even in the absence of documented change; for example perhaps certain aspects of LC microarchitecture will prove to confer biomechanical susceptibility for a given individual eye. One manner of probing biomechanical behavior of ONH tissues is by acute “compliance test” whereby IOP is manipulated acutely to alter mechanical load and the response of ONH structures is imaged *in vivo*.(Agoumi et al., 2011; Burgoyne et al., 1995; Coleman et al., 1991; Fortune et al., 2011; Heickell et al., 2001; Strouthidis et al., 2011a) This kind of study is also important for characterizing the degree to which structural parameters are influenced by the ambient IOP level in order to help inform cross-sectional clinical diagnosis.(Fortune et al., 2009) Thus it may be that through a combination of “baseline” ONH structural parameters and acute compliance test results, the biomechanical integrity of ONH tissues will refine predictions of which individual eyes are at greatest risk for developing glaucoma and the most rapid rate of progression.

One more important way of characterizing ONH structure is the quantitative measurement of the neural rim tissue. For more than two decades, CSLT was the predominant means by which reliable clinical measurements of ONH structural parameters such as rim width or rim area were obtained.(Alencar et al., 2008, 2005; Sharma et al., 2008; Wollstein et al., 2000; Zangwill et al., 2013; Zangwill et al., 2005) The preceding sections of this review alluded to the capability of CSLT for measuring ONH surface topography, that is, providing a high-resolution 2D map of “surface height” relative to an axial (longitudinal) reference plane. By outlining within that map the outer extent of the optic disc and by determining where the surface dips below the reference plane (i.e. designating the border between the rim and the “optic cup”), the dimensions of the optic disc rim tissue can be calculated with high precision.(2005) For example, Shimazawa et al monitored rim (and cup) parameters longitudinally using CSLT in cynomolgus monkeys with very high IOP over 12–16 weeks

and found high correlations with RNFL parameters determined both by scanning laser polarimetry (SLP) and by histological measurements.(Shimazawa et al., 2006) However, there was no means of IOP control at the time of CSLT scanning in order to account for the elastic (in contrast to plastic) components of ONH deformation.(Burgoyne et al., 1995; Coleman et al., 1991; Heickell et al., 2001) Since peripapillary SLP measurements are minimally affected by ambient IOP,(Fortune et al., 2009) correlations may be even higher than reported. Yucel and colleagues reported strong correlations between ONH parameters measured using CSLT and optic nerve axon counts from eyes of macaque monkeys with EG,(Yucel et al., 1998) yet again these correlations may have been even stronger after accounting for the effects of ambient IOP at the time of the CSLT scans.(Burgoyne et al., 1995; Coleman et al., 1991; Heickell et al., 2001; Yucel et al., 1998) Hare et al demonstrated evidence of a protective effect from memantine treatment in monkeys with EG based on longitudinal CSLT measurements of ONH structure.(Hare et al., 2004)

However, it is well known that the lack of a stable, reliable reference plane ultimately hampers both the precision and accuracy of CSLT measurements and their ability to detect ONH structural changes in human glaucoma.(Kamal et al., 2000; Strouthidis et al., 2005a; Strouthidis et al., 2005b) Studies have also shown that agreement between CSLT and expert analysis of stereoscopic photographs for detecting progressive ONH structural change is limited.(O'Leary et al., 2010; Vizzeri et al., 2010; Wollstein et al., 2000) Hence there is growing interest in application of OCT for the measurement of ONH neural rim parameters since OCT provides a more accurate anatomical definition of rim tissue boundaries and more stable anatomical reference plane (for review, see(Chauhan and Burgoyne, 2013)). Specifically, given the advantage of cross-sectional imaging with high axial resolution, OCT is able to provide neural rim measurements that better follow ONH anatomy, such as those based on the minimum distance calculations.(Chauhan et al., 2013; Chen, 2009; Gardiner et al., 2014; Povazay et al., 2007) In addition to neural rim measurements such as minimum rim width, minimum rim area and rim volume, OCT also should be capable of producing 2D surface topography maps with resolution equal to CSLT since increasingly fast acquisition speeds (now into the MHz range for research instruments) will enable high density A-scan patterns with minimal eye movement artifact.

Strouthidis et al first demonstrated in a longitudinal study of NHP EG that minimum rim width and minimum rim area measured using SDOCT had decreased from baseline at the onset of CLST-detected ONH surface topography change. Evaluating entire longitudinal sequences, He et al(He et al., 2014) subsequently demonstrated that neural rim thinning as measured by these SDOCT parameters preceded or coincided with CSLT-detected ONH surface topography change in most NHP EG eyes. Based on SDOCT data from a similar NHP EG model, as well as cross-sectional analyses of clinical data from human eyes, Patel et al also reported evidence that neural rim thinning precedes peripapillary RNFL thinning. (Patel et al., 2014) What remains to be determined is the extent to which ONH rim deformation and thinning relates directly to ONH connective tissue deformation and remodeling since current evidence from NHP EG suggests that early-stage changes of both structural components manifest in concert before any decrease in the total number of optic nerve axon loss occurs. Figure 1 provides an individual example from NHP EG of

relationships between SDOCT derived ONH parameters, peripapillary RNFL thickness and complete orbital optic nerve axon counts.

Another desirable ONH imaging target is blood flow. Longitudinal studies by Lin Wang and colleagues using laser speckle flowgraphy have demonstrated that blood flow through ONH capillary beds actually increases above normal during the earliest stages of NHP EG, followed by progressive decline in proportion to the degree of peripapillary RNFL thinning. (Cull et al., 2013) Further, their studies have revealed that the dynamic (but not the static) autoregulation of ONH capillary blood flow is altered in NHP EG.(Wang et al., 2014b; Wang et al., 2014c) Future studies should determine how ONH capillary bed blood flow changes relate to ONH structural changes such as deformation and remodeling of LC microarchitecture, LC insertion and neural rim thinning.

As in human glaucoma and the NHP EG model, it is thought that the site of injury initiating subsequent RGC axon degeneration and death in rodent EG models is also located within the ONH)(Chidlow et al., 2011; Howell et al., 2007; Jakobs et al., 2005; Martin et al., 2006; Morrison et al., 1997; Salinas-Navarro et al., 2010; Schlamp et al., 2006; Soto et al., 2008; Soto et al., 2011) Therefore the ONH is an important target for *in vivo* imaging in small rodents. Chauhan and colleagues reported the first longitudinal study demonstrating ONH changes *in vivo* in a rodent model of EG.(Chauhan et al., 2002) Using CSLT, Chauhan and colleagues documented progressive “cupping” of the rat ONH in proportion to the degree of IOP elevation and in some cases also a dramatic expansion of the scleral canal confirmed histologically. Guo et al applied longitudinal CSLO and OCT imaging in a similar EG model in rats and confirmed the development of ONH changes in vivo, including expansion of the scleral canal.(Guo et al., 2005) Interestingly, Chauhan et al presented evidence for a “threshold” of peak IOP and IOP integral beyond which these ONH changes observed *in vivo* became increasingly prominent.(Chauhan et al., 2002) However, they also reported that the proportion of surviving axons exhibited a more linear relationship to peak and integral IOP, suggesting that the sudden, dramatic structural changes in the rat ONH in that EG model may reflect changes in connective tissues like the peripapillary sclera and may be “primarily a mechanical phenomenon”.(Chauhan et al., 2002) The full-field ERG results presented in the study by Chauhan et al suggest retinal ischemia was also present above the same IOP threshold that caused rapid severe cupping and expansion of the scleral canal.(Bui et al., 2013; Bui et al., 2005; Bui and Fortune, 2004; Fortune et al., 2004) Thus it may be that ocular ischemia in combination with significant chronic IOP elevation combine to create a more dramatically altered mechanical environment in the rat (or any) ONH.

Early demonstrations of OCT imaging in small rodents using SDOCT operating at either 830 nm (and bandwidth of 70 nm),(Ruggeri et al., 2007) at 870 nm (bandwidth of 100 nm) (Fischer et al., 2009) or at 900 nm with ultrahigh-resolution (bandwidth of 150 nm) (Srinivasan et al., 2006) revealed the difficulty of imaging details of the deeper ONH structures, which are largely masked in shadows cast by the overlying dense vasculature. Thus few studies have used OCT specifically to assess ONH structure in rodents. Fortune et al documented rapid and reversible deformation of ONH and peripapillary tissue in the rat eye subjected to acute IOP elevation using a commercial SDOCT system (Heidelberg Spectralis operating at 870 nm with 100 nm bandwidth).(Fortune et al., 2011) Based on the

limited visibility of deeper ONH structures in that study,(Fortune et al., 2011) a subsequent study was performed in healthy naïve rats, which showed that SDOCT imaging at 1050 nm with the EDI mode enhanced visibility of deeper ONH structures in the rat eye.[Choe et al., *Invest Ophthalmol Vis Sci* 2012;53: E-Abstract 2820] Images through the ONH of mice shown recently in reports using another commercial SDOCT system (Bioptigen) suggest that assessment of ONH structure may be possible with that system, though the investigators in those studies were focused on the peripapillary retina and did not comment on the ONH.(Liu et al., 2014; Yang et al., 2012b) Using a custom SDOCT system operating at 1300 nm in combination with their ultra-high sensitive optical microangiography technique, Zhi and colleagues have demonstrated extraordinary capabilities to visualize detailed anatomy of the rat ONH *in vivo*, especially of the microvasculature and responses to acute IOP elevation.(Zhi et al., 2011; Zhi et al., 2012) Polarization-sensitive OCT may further enhance visualization of connective tissues and other birefringent structures in the rat eye, such as the peripapillary sclera as recently demonstrated by Baumann et al.(Baumann et al., 2014) For the rodent ONH, which lacks a collagenous LC, an approach such as polarization-sensitive OCT may enable *in vivo* detection of changes in the “glial LC”, including density and orientation of astrocyte processes and their actin cytoskeleton.(Lye-Barthel et al., 2013; Sun et al., 2013; Tehrani et al., 2014) Implementation of AO strategies for overcoming challenges inherent to imaging rat and especially mouse eyes by OCT (and SLO) may also become important to ONH assessment in EG models.(Geng et al., 2012; Geng et al., 2009; Jian et al., 2013);Jian et al., *Invest Ophthalmol Vis Sci* 2014;55: E-Abstract 2083;*Zhang et al., Invest Ophthalmol Vis Sci* 2014;55: E-Abstract 2085.

2. Imaging the RNFL

Ultimately, glaucoma causes degeneration of RGC axons, which are visible along the innermost layer of the retina by ophthalmoscopy and other techniques. For decades RNFL defects have been considered an important diagnostic sign of glaucoma since they present clinically at an early stage and are predictive of subsequent visual field loss.(Hoyt et al., 1973; Hoyt and Newman, 1972; Sommer et al., 1991) The visibility of axon bundles within the RNFL by clinical ophthalmoscopy and photography depends on their reflectance, which is also known to be highly directional, wavelength dependent, and strongly influenced by normal cytoskeletal integrity.(Huang et al., 2006; Knighton and Huang, 1999; Knighton et al., 1989; Knighton and Qian, 2000; Knighton and Zhou, 1995; Zhou and Knighton, 1997)

However, the minimum loss of RNFL detectable by traditional clinical methods such as ophthalmoscopy and photography may be 50 to 70 μm, or as much as 50% of the normal thickness.(Quigley, 1986; Quigley and Addicks, 1982) Direct clinical examination and photography are also limited by subjectivity, with high intra- and inter-observer variability. More recent development of advanced techniques for imaging the RNFL have enabled reliable, sensitive and quantitative measurements to be obtained clinically with the hope of improving glaucoma detection and management.(Greaney et al., 2002; Medeiros et al., 2004; Townsend et al., 2009; Zangwill and Bowd, 2006) The two techniques that have been used most commonly for this purpose are SLP(Lemij and Reus, 2008; Medeiros et al., 2007; Reus and Lemij, 2004; Weinreb et al., 1990) and OCT,(Schuman et al., 1995; Wollstein et

al., 2005b) both of which provide predictive capability for future glaucoma progression including loss of vision.(Lalezary et al., 2006; Mohammadi et al., 2004)

Based on the principle of interferometry, OCT produces high-resolution cross-sectional images of tissue structure,(Costa et al., 2006; Drexler and Fujimoto, 2008; Huang et al., 1991) which can be used to estimate thickness of individual retinal layers such as the RNFL by automatic detection of the relatively steep reflectance transitions at its anterior and posterior boundaries.(Sakamoto et al., 2010) RNFL thickness measurements obtained by OCT have been shown to agree with histomorphometric measurements of RNFL thickness (Schuman et al., 2007) and optic nerve axon counts (Cull et al., 2012, 2014; Fortune et al., 2015) in NHP EG and in rats after optic nerve crush injury.(Nagata et al., 2009) RNFL thickness measurements from OCT also correlate with RGC soma counts obtained in vivo by CSLO in mice and rats after optic nerve injury.(Chauhan et al., 2012; Choe et al., 2014)

In contrast, SLP measures the relative phase retardance of orthogonally polarized states of its imaging source after a double pass through the tissue sample.(Weinreb et al., 1990) The relatively high phase retardance exhibited by the RNFL reflects form birefringence, an optical property thought to be due to the orderly parallel array of thin cylindrical cytoskeletal components within these axons, including microtubules and neurofilaments. (Huang and Knighton, 2002, 2005; Zhou and Knighton, 1997) Empirical evidence published over the past decade supports this theoretical framework.(Fortune et al., 2008b; Huang and Knighton, 2005; Pocock et al., 2009) Thus measurements of RNFL birefringence might well provide a sensitive biomarker of compromised cytoskeleton integrity within RGC axons. (Fortune et al., 2008b; Huang et al., 2004; Huang and Knighton, 2005) The importance of this idea is underscored by evidence of axonal cytoskeletal changes observed in models of EG models, including their earliest stages;(Balaratnasingam et al., 2008; Balaratnasingam et al., 2007; Fortune et al., 2014a; Huang et al., 2011a; Huang and Knighton, 2009; Kashiwagi et al., 2003) some of which may represent mechanisms of further susceptibility.(Beirowski et al., 2010; Coleman, 2005; Soto et al., 2011; Vickers et al., 1995)

RNFL birefringence can be assessed in a clinical setting either directly, such as by polarization-sensitive OCT(Braaf et al., 2014; Cense et al., 2002, 2004; Cense et al., 2007; Dwelle et al., 2012; Elmaanaoui et al., 2011; Gotzinger et al., 2005; Pircher et al., 2011; Rylander et al., 2005; Zotter et al., 2013) or it can be inferred by comparing SLP measurements of RNFL retardance to OCT measurements of RNFL thickness. For example, a series of experiments by Fortune and colleagues provides clear evidence of an early stage of RGC degeneration when both axonal cytoskeletal abnormalities and RGC functional abnormalities are found in the absence of significant thinning of axon bundles within the RNFL in an NHP model of EG and after optic nerve transection.(Fortune et al., 2013a; Fortune et al., 2012; Fortune et al., 2008a) (Fortune et al., 2015; Fortune et al., 2014a). As mentioned, the reflectance of axons within the RNFL is also thought to depend on the integrity of their cytoskeleton.(Huang et al., 2006; Knighton et al., 1998) Thus it is interesting that both clinical(van der Schoot et al., 2012; Vermeer et al., 2012) and laboratory studies (Huang et al., 2011b) have demonstrated altered reflectance (and/or attenuation) of the glaucomatous RNFL, suggesting that this phenomenon might be another

sensitive indicator of early axonal damage and a target for novel clinical imaging strategies. (Zhang et al., 2011)

In a laboratory setting, the visibility of RNFL axons for in vivo imaging can be further enhanced by introduction of exogenous fluorescent contrast agents(Abbott et al., 2013; Kanamori et al., 2012; Kanamori et al., 2010) or genetically-expressed fluorescent reporters. (Leung et al., 2011; Walsh and Quigley, 2008) The addition of AO to compensate for optical aberrations enables imaging of RNFL structure in exquisite detail, with or without fluorescent contrast agents by SLO, or by OCT, including in the shorter eyes of small rodents.(Geng et al., 2012; Geng et al., 2009; Gray et al., 2008; Jian et al., 2013);[Jian et al., *Invest Ophthalmol Vis Sci* 2014;55: E-Abstract 2083;*Zhang et al., Invest Ophthalmol Vis Sci* 2014;55: E-Abstract 2085] AO-SLO and AO-OCT have recently been used to image RNFL bundles in human eyes, revealing fine detail in both healthy and damaged areas.(Chen et al., 2015; Huang et al., 2014; Kocaoglu et al., 2011; Kocaoglu et al., 2014b; Takayama et al., 2012; Takayama et al., 2013b) One interesting finding common to several of these recent AO studies is that reflectivity of RNFL bundles is often discrete, certainly more so than can be appreciated without AO (e.g., see Figure 2). It is possible that these more discrete reflectivity profiles arise from the varicosities known to be present along RGC axons within the RNFL, most commonly at the site of internal mitochondria.(Wang et al., 2003) Mitochondria are known to be actively transported along these unmyelinated axon segments and that this process is disturbed in a rodent EG model.(Brown, 2003)[Takihara et al., *Invest Ophthalmol Vis Sci* 2013;54: E-Abstract 756 and 2014;55: E-Abstract 2408] These findings lead to the sound prediction that some aspects of RNFL bundle reflectivity might be dynamic and related to transport activity. Huang and colleagues have recently demonstrated in a rat retinal explant preparation that the discrete speckle pattern of RNFL reflectance was dynamic and related to activity.(Huang et al., 2013) It should be possible to extend these developments to investigations of RGC axonal activity in the living eye, in humans and in EG models, given 3D cellular-level resolution and MHz speed of recent AO-OCT systems. (Kocaoglu et al., 2014b) Figure 3 shows preliminary supporting evidence from recent work by Liu, Kocaoglu, Miller and colleagues using MHz AO-OCT.(Kocaoglu et al., 2014b)

Meanwhile, to date, the application of imaging methods such as SLO and OCT to perform longitudinal in vivo assessment of RNFL damage in models of optic nerve injury including EG has been primarily focused on quantification of RNFL (or total retinal) thickness. As mentioned above, progressive loss of RNFL thickness is a well-established outcome measure in NHP models of EG.(Cull et al., 2013; Cull et al., 2012; Fortune et al., 2013a; Fortune et al., 2012; Fortune et al., 2015; Fortune et al., 2008a; Fortune et al., 2014b; Fortune et al., 2013b; He et al., 2014; Patel et al., 2014; Strouthidis et al., 2011b; Yang et al., 2014) Such measurements are also becoming increasingly applied in rodent models. Kawaguchi et al inferred the thickness of the RNFL from changes in the focal plane setting of an SLO and documented a specific decline after optic nerve crush in rats.(Kawaguchi et al., 2006) Nagata et al showed that OCT measurements of RNFL thickness declined progressively after optic nerve crush in rats and were strongly correlated to histological measurements of RNFL thickness.(Nagata et al., 2009) Gabriele et al measured total retinal thickness by SDOCT and found an initial increase, followed by progressive decline after

optic nerve crush in mice.(Gabriele et al., 2011) Chauhan et al measured both RGC density and total retinal thickness in vivo, by CSLO and SDOCT respectively, after optic nerve transection in mice and showed progressive decline of both parameters.(Chauhan et al., 2012) Choe et al measured RNFL thickness and RGC density in vivo by SDOCT and CSLO, respectively, and found a strong correlation between them over 4 weeks of longitudinal follow up after optic nerve transection in rats.(Choe et al., 2014) Though Choe et al also reported that RNFL thinning was delayed relative to the onset of declining RGC soma, similar to what Nakano et al reported earlier for NMDA-induced injury.(Nakano et al., 2011) Liu et al used longitudinal SDOCT imaging to document a progressive decline in the combined thickness of the RNFL, RGC layer and inner plexiform layer (IPL) after optic nerve crush in mice and also found that this combined layer thickness measurement was correlated to density of soma in the RGC layer and progressive functional loss measured by ERG.(Liu et al., 2014)

Guo et al were the first to report SDOCT measurements of retinal layer thicknesses in a rodent EG model based on chronic IOP elevation.(Guo et al., 2010) They found a small decrease in RNFL thickness 3- and 8-weeks after IOP elevation was induced, but no change in the thickness of the IPL and a rather substantial progressive loss of outer retinal thickness that is not observed in human glaucoma(Ishikawa et al., 2005; Tan et al., 2009; Wang et al., 2009) or in NHP models.[Wilsey et al., *Invest Ophthalmol Vis Sci* 2015;56: E-Abstract 638] Yang et al also reported that in a mouse EG model based on chronic IOP elevation, loss of the combined RNFL, RGC and IPL thickness measured by SDOCT was related to RGC density sampled histologically.(Yang et al., 2012b) Gramlich et al found after chronic recurrent episodes of a short-duration IOP “spike” (1 hour each to 30–35 mmHg), there was a decline in total retinal thickness measured by SDOCT and RGC density measured histologically as well as an increase in the optic nerve axon damage grade.(Gramlich et al., 2014) Using longitudinal SDOCT imaging, Abbott et al found that RNFL loss occurred earlier and was more severe in older rats age 9.5-months as compared with younger rats aged 2-months despite similar exposure to chronic IOP elevation over 3-weeks. Abbott et al also reported that axonal transport disruption and optic nerve damage were substantially worse than RNFL thinning, especially in the older rats and confirmed by post mortem microscopy of retinal whole mounts that there was relative preservation of the intraretinal portion of RGC axons. This underscores both the usefulness and limitations of in vivo imaging and the need to continue characterizing the relationship between RNFL thickness and the integrity of distal axon segments.(Crish et al., 2010; Cull et al., 2012; Howell et al., 2007; Huang et al., 2011b; Schlamp et al., 2006)

Figure 4 shows an example of longitudinal imaging by CSLO and SDOCT (Spectralis HRA +OCT, Heidelberg Engineering, GmbH) in a pigmented rat during baseline and four weekly follow-ups after unilateral optic nerve transection.(Choe et al., 2014) Infrared reflectance images obtained by CSLO are shown at one baseline time point in panel A and at follow-up time points 1, 2 and 4 weeks after transection in panels B, C and D, respectively. The RNFL bundle reflectance has nearly completely disappeared by 4-weeks while the contrast of the major retinal vessels and capillaries has become more prominent against the fundus background. The horizontal yellow line in panel A shows the location of one of 290 raster

lines from the SDOCT volume, the corresponding B-scan is shown in panel E for baseline and E' 4-weeks after transection; similarly, the vertical yellow line shown in panel A indicates the position of an interpolated B-scan, which is shown in panel F for baseline and F' 4-weeks after transection. Note the nearly complete thinning of the RNFL 4 weeks after transection as compared with baseline (indicated by the green arrows). En face projections from the SDOCT volumes obtained for the entire longitudinal series are shown for the transected eye in row G and the fellow control eye in row H. The RNFL progressively disappears over weeks 2–4 in the transected eye. In EG models, at least in those where the optical media remain clear enough to obtain image series like these, it will be interesting to test hypotheses about longitudinal changes in RNFL reflectance and thickness relative to the underlying changes in axon ultrastructure.(Fortune et al., 2014a)

3. Imaging the RGC Soma and Dendrites

As first demonstrated by Zeimer and colleagues, in vivo imaging of the macula offers an important, complementary approach to glaucoma clinical care and research.(Zeimer et al., 1998) Since loss of RGCs will result not only in thinning of the RNFL, but also of the inner retina, imaging the clinical macula by OCT has gained attention for its potential diagnostic capability.(Greenfield et al., 2003; Hood et al., 2013; Hood et al., 2014; Ishikawa et al., 2005; Leung, 2014; Lisboa et al., 2013; Moreno et al., 2011; Rao et al., 2013; Raza et al., 2011; Tan et al., 2009; Wang et al., 2009) Although most studies show that diagnostic power is not any better than that achieved using a much simpler measurement of peripapillary RNFL thickness(Lisboa et al., 2013; Moreno et al., 2011; Rao et al., 2013; Tan et al., 2009) – and notwithstanding that macular measurements will generally require longer scan times and more involved segmentation – there is likely an important role for macular imaging in clinical glaucoma management, at least in detection of damage missed by standard visual field and OCT testing or confirmation of otherwise questionable defects.(Hood et al., 2013; Hood et al., 2014; Leung, 2014) Like that of the human retina, RGC density also increases dramatically near the fovea of nearly all other primates, so OCT imaging of the macula also proves useful for detection of glaucomatous damage in NHP EG models.(Luo et al., 2014) [Wilsey et al., *Invest Ophthalmol Vis Sci* 2015;56: E-Abstract 638] Luo and colleagues showed that localized measurements of macular inner retinal thickness (combined RGC +IPL) were correlated with multifocal ERG measurements of RGC function in a NHP EG model.(Luo et al., 2014) Similarly, our group has reported that macular retinal structural and functional losses are correlated and specific to RGCs over a wide range of severity in NHP EG (Figure 5). Consistent with an earlier observation by Ishikawa et al,(Ishikawa et al., 2005) we also found that outer retinal thickness in the macular was slightly *increased* in NHP EG, though that subtle effect was only weakly related to EG severity.[Wilsey et al., *Invest Ophthalmol Vis Sci* 2015;56: E-Abstract 638]

Because layer-by-layer segmentation is more challenging for the thinner inner retina of small rodents, it has been common for investigators to evaluate either total retinal thickness or the combined RNFL+RGC+IPL thickness (often referred to as the ganglion cell complex, GCC) using OCT measurements in these species.(Fortune et al., 2011; Gabriele et al., 2011; Gramlich et al., 2014; Guo et al., 2010; Liu et al., 2014; Lozano and Twa, 2013; Nakano et al., 2011; Yang et al., 2012b) OCT measurements of specific inner retinal layer thickness

(such as RNFL) in rodents has generally been limited to isolated spatial samples or to single circular B-scans around the ONH.(Abbott et al., 2014a; Abbott et al., 2014b; Chauhan et al., 2012; Choe et al., 2014; Fortune et al., 2011; Guo et al., 2010; Nagata et al., 2009)

However, anticipating improved accuracy and speed of forthcoming automated segmentation algorithms, such as recently demonstrated by Antony et al(Antony et al., 2013) and Srinivasan et al,(Srinivasan et al., 2014) it should be soon be feasible to address persisting questions about glaucoma pathogenesis in EG models (perhaps also clinically in humans) using in vivo imaging. For example, one aspect of glaucoma pathogenesis receiving renewed attention is RGC dendritic atrophy.(Chong and Martin, 2014; Leung et al., 2011; Li et al., 2011; Morgan, 2012) Weber and colleagues(Weber et al., 1998) first reported on the basis of cross-sectional data that degenerative retraction of the dendritic arbor preceded thinning of axon caliber or shrinkage of the RGC soma in a NHP EG model, though these findings all occurred well after deformation of the ONH, consistent with the hypothesis that initial RGC injury occurs within the ONH with subsequent degenerative morphological changes. Shou et al subsequently reported similar cross-sectional observations of dendritic atrophy in a feline model of EG.(Shou et al., 2003) More recently, Williams et al(Williams et al., 2013) reported evidence that RGC dendritic atrophy occurs prior to significant axon degeneration in the DBA/2J mouse model of heritable glaucoma, again on the basis of cross-sectional data. If dendritic atrophy occurs during early stages of the glaucomatous RGC injury in humans, its detection by clinical imaging could serve as a warning sign to advance therapy (IOP lowering or other novel mechanism). Similarly, as with the other target structures discussed in this review, in vivo imaging also can be applied in EG models for hypothesis testing and for refining relevance to human glaucoma. Particularly interesting within the context of imaging RGC dendritic integrity in vivo is the recent demonstration by Tanna and colleagues(Tanna et al., 2010) that the improved axial resolution afforded by a commercial broadband SDOCT instrument was sufficient to detect sublamina within the IPL. Meanwhile, evidence based on current clinical OCT imaging is equivocal in terms of whether the phenomenon of dendritic atrophy occurs in human glaucoma and/or whether it can be detected prior to thinning of RGC axon bundles or loss of RGC soma.(Hood et al., 2013; Leung, 2014; Lisboa et al., 2013; Moreno et al., 2011; Rao et al., 2013; Tan et al., 2009).

Nakano et al found by SDOCT thinning of the GCC was delayed relative to the decrease in RGC soma density after NMDA-induced injury in mice. Choe et al reported a similar delay between RNFL thickness and RGC density in the first week after optic nerve transection in rats.(Choe et al., 2014) Using longitudinal CSLO imaging *in vivo*, Leung et al have shown numerous examples of RGC somas persisting longer than their axons after optic nerve crush. (Leung et al., 2011) The report by Leung et al also demonstrated clearly that dendritic tree shrinkage was consistently the earliest morphological change detectable by *in vivo* imaging after crush injury.(Leung et al., 2011) Few studies of EG based on chronic IOP elevation have specifically addressed this question. Guo et al observed greater loss of outer retinal layer thickness than for RNFL, IPL or GCC in a rat EG model. Our group has observed in a NHP EG model that loss of macular inner retinal layer thickness is correlated with loss of peripapillary RNFL thickness, but a slight increase in macular outer retinal layer thickness

was unrelated to EG severity (Fig. 5). Future studies aim to evaluate the temporal sequence of inner retinal layer changes as compared with ONH changes and axon loss.

While OCT measurements of individual retinal layer morphology and thickness can be done both in the clinic and laboratory, it is not yet possible to image individual RGCs in human eyes. In the laboratory, however, various techniques for visualizing RGCs *in vivo* have evolved over the past two decades. Generally such techniques involve imaging by either epifluorescence microscopy,(Naskar et al., 2002; Thanos et al., 2002) fundus photography(Murata et al., 2008), intravital confocal microscopy (Sabel et al., 1997; Thanos, 1991; Walsh and Quigley, 2008) or CSLO(Abbott et al., 2013; Chauhan et al., 2012; Choe et al., 2014; Cordeiro et al., 2004; Geng et al., 2012; Geng et al., 2009; Gray et al., 2008; Higashide et al., 2006; Kanamori et al., 2012; Leung et al., 2008a; Leung et al., 2008b; Leung et al., 2011; Nakano et al., 2011) after introduction of a fluorescent tracer via retrograde transport from the midbrain(Abbott et al., 2013; Choe et al., 2014; Gray et al., 2008; Higashide et al., 2006; Kanamori et al., 2012; Murata et al., 2008; Prilloff et al., 2010; Sabel et al., 1997; Thanos, 1991; Thanos et al., 2002) or a fluorescent reporter molecule whose expression is driven by a promoter that is relatively specific to RGCs.(Chauhan et al., 2012; Geng et al., 2012; Geng et al., 2009; Leung et al., 2008a; Leung et al., 2008b; Leung et al., 2011; Murata et al., 2008; Nakano et al., 2011; Walsh and Quigley, 2008) In some transgenic lines such as the Thy-1 YFP mouse, expression is limited to a small enough proportion of RGCs to enable visualization *in vivo* of even fine dendritic structure by CSLO. (Leung et al., 2011; Walsh and Quigley, 2008) Use of SLO with AO to compensate for optical aberrations has also enabled visualization *in vivo* of RGC fine dendritic structure. (Geng et al., 2012; Geng et al., 2009; Gray et al., 2008) Though several of these previous studies have demonstrated decline in RGC density, changes in RGC soma size, dendritic arbor and axonal integrity, or RGC apoptosis after optic nerve injury,(Chauhan et al., 2012; Choe et al., 2014; Cordeiro et al., 2004; Higashide et al., 2006; Kanamori et al., 2012; Leung et al., 2008b; Leung et al., 2011; Murata et al., 2008; Nakano et al., 2011; Naskar et al., 2002; Prilloff et al., 2010; Sabel et al., 1997; Thanos et al., 2002) none has yet to evaluate longitudinal changes in an EG model that adequately recapitulates the human disease. It is anticipated that such studies will emerge in the near future.

4. Future Directions

As reviewed above, one distinct advantage of OCT over other imaging modalities is its superior axial resolution. However, one advantage that SLO (confocal or flood illuminant) imaging has over OCT is the capability for fluorescence detection, which can be combined with molecular tags or reporters to reveal fine structure or pathological events. During the past decade, interest has grown in the development of contrast agents for enhancement of OCT signals with the goal of targeting specific molecular markers that could transform diagnostic and/or therapeutic approaches.(Boppart et al., 2005; Gordon and Jayagopal, 2014; Jung et al., 2011; Troutman et al., 2007) Gold nanorods (GNRs) have emerged as an excellent candidate due to the biocompatible nature of gold, the ability to functionalize gold particles for covalent binding to specific ligands for molecular targeting and to their inherent physical property of surface plasmon resonance, which can be readily tuned to a specific frequency by controlling rod dimensions during synthesis.(Troutman et al., 2007) Safe and

effective use of GNRs *in vivo* as a contrast agent for OCT has already been demonstrated using photothermal OCT.(Jung et al., 2011; Tucker-Schwartz et al., 2014; Tucker-Schwartz et al., 2012) Wang et al reported use of GNRs in an *ex vivo* ocular perfusion system to visualize otherwise silent flow fields within the anterior chamber by Doppler OCT.(Wang et al., 2014a) De la Zerda et al reported visualization of signal enhancement by reflectance OCT *in vivo* after injecting GNRs into the corneal stroma in mice.(de la Zerda et al., 2014) Sandrian et al(Gabriele Sandrian et al., 2012) attempted to introduce into the retina GNRs conjugated to the Thy1 antibody for targeted binding to RGCs, but found that intravitreally injected GNRs became trapped within inflammatory cells and networks within the vitreous; GNRs were not observed within RGCs and the retinal OCT signal was severely attenuated. Thus an important obstacle toward realization of this goal is the ability to get GNRs to cross the retinal internal limiting membrane (ILM) in order to achieve targeted retinal cell binding. Once realized, multimodal imaging approaches such as combined AO-SLO and AO-OCT(Felberer et al., 2014; Zawadzki et al., 2011) could be used in conjunction with combined constructs for contrast enhancement and molecular tagging (such as GNRs conjugated with fluorescent antibodies) to visualize pathophysiological changes in vivo at the molecular level. Other recent exciting work has demonstrated that light responses from individual RGCs can be quantified by in vivo imaging in the living mouse and macaque eye. (Yin et al., 2013; Yin et al., 2014) Other multimodal approaches such as Multifunctional OCT(Hong et al., 2014) or combining polarization-sensitive OCT with AO(Cense et al., 2009) offer further promise for hypothesis testing and clinical diagnostics. Finally, the speed of OCT acquisition continues to increase rapidly, reaching extraordinary capacity such as that recently demonstrated by Klein et al.(Klein et al., 2013) These and other developments should surely facilitate future discovery of key pathogenic events in glaucoma and other diseases of the eye as well as targets for novel therapeutic intervention.

5. Summary and Conclusions

The phrase “bench-to-bedside” is often used to describe the translation of laboratory discovery into clinical care, for the enterprise of improving understanding of human health and disease through the use of experimental models. Technologies for in vivo ocular imaging are one important aspect of conducting such studies. They provide outcome measures such as anatomical parameters that can be used in both settings: laboratory studies in animal models and clinical research in human patients. Indeed, it is possible that failure to deliver a viable option for neuroprotection in glaucoma is due in part to the lack of commonality between the outcome measures used in pre-clinical studies in animals (typically post mortem histological measures such as RGC counts) and those acceptable for clinical research and randomized clinical trials. For example, maintaining RGC soma counts in an animal model may not translate to preservation of vision if surviving RGCs do not each maintain a viable, functioning axon that correctly conveys signals to its central target. (Raff et al., 2002; Whitmore et al., 2005) Moreover, without common outcome measures it is difficult to compare the pathophysiological sequence of an experimental model with the human disease, to ensure relevance and/or refine any given model accordingly. Thus by incorporating in vivo imaging into laboratory studies, the glaucoma research community can not only reduce the number of animals needed to achieve robust outcomes, but also refine and prove relevance of EG models to hasten the translation of discovery from bench-to-

bedside. Ironically, most of the recent spectacular achievements in ophthalmic imaging have been developed in for use in human beings and need to be adapted for use in laboratory animals, rather like bedside-to-bench translation. Yet in order to extend the limitations of current imaging paradigms to provide adequate contrast, spatial and temporal resolution for assessment of cellular and subcellular structure and function of RGCs *in vivo* and to identify specific cellular and molecular targets for imaging in vivo, future translational research will need to occur in both directions.

Acknowledgments

The author would like to express sincere gratitude to the many mentors and collaborators whose generosity, friendship and hard work have contributed to my own ability to maintain engagement in the rewarding field of glaucoma research. Among them, several in particular warrant special mention, including current collaborators Claude Burgoyne, Juan Reynaud, Grant Cull, Lin Wang, Shaban Demirel, Bang Bui, Stuart Gardiner, Steven Mansberger and Hongli Yang as well as long-standing mentors Jack Cioffi, Don Hood and Chris Johnson. The author would also like to thank Galen Williams, Christy Hardin and Luke Reyes for their enthusiastic support and expert technical assistance in conducting recent and ongoing laboratory experiments.

Financial Support: NIH R01-EY019327, Legacy Good Samaritan Foundation

References

Abbott CJ, Choe TE, Burgoyne CF, Cull G, Wang L, Fortune B. Comparison of Retinal Nerve Fiber Layer Thickness In Vivo and Axonal Transport after Chronic Intraocular Pressure Elevation in Young versus Older Rats. PLoS One. 2014a; 9:e114546. [PubMed: 25501362]

Abbott CJ, Choe TE, Lusardi TA, Burgoyne CF, Wang L, Fortune B. Imaging axonal transport in the rat visual pathway. Biomed Opt Express. 2013; 4:364–386. [PubMed: 23412846]

Abbott CJ, Choe TE, Lusardi TA, Burgoyne CF, Wang L, Fortune B. Evaluation of retinal nerve fiber layer thickness and axonal transport 1 and 2 weeks after 8 hours of acute intraocular pressure elevation in rats. Invest Ophthalmol Vis Sci. 2014b; 55:674–687. [PubMed: 24398096]

Agoumi Y, Sharpe GP, Hutchison DM, Nicolela MT, Artes PH, Chauhan BC. Laminar and prelaminar tissue displacement during intraocular pressure elevation in glaucoma patients and healthy controls. Ophthalmology. 2011; 118:52–59. [PubMed: 20656352]

Akagi T, Hangai M, Takayama K, Nonaka A, Ooto S, Yoshimura N. In vivo imaging of lamina cribrosa pores by adaptive optics scanning laser ophthalmoscopy. Invest Ophthalmol Vis Sci. 2012; 53:4111–4119. [PubMed: 22669726]

Alencar LM, Bowd C, Weinreb RN, Zangwill LM, Sample PA, Medeiros FA. Comparison of HRT-3 glaucoma probability score and subjective stereophotograph assessment for prediction of progression in glaucoma. Invest Ophthalmol Vis Sci. 2008; 49:1898–1906. [PubMed: 18436823]

Anderson DR, Hendrickson A. Effect of intraocular pressure on rapid axoplasmic transport in monkey optic nerve. Invest Ophthalmol. 1974; 13:771–783. [PubMed: 4137635]

Antony BJ, Abramoff MD, Harper MM, Jeong W, Sohn EH, Kwon YH, Kardon R, Garvin MK. A combined machine-learning and graph-based framework for the segmentation of retinal surfaces in SD-OCT volumes. Biomed Opt Express. 2013; 4:2712–2728. [PubMed: 24409375]

Balaratnasingam C, Morgan WH, Bass L, Cringle SJ, Yu DY. Time-dependent effects of elevated intraocular pressure on optic nerve head axonal transport and cytoskeleton proteins. Invest Ophthalmol Vis Sci. 2008; 49:986–999. [PubMed: 18326722]

Balaratnasingam C, Morgan WH, Bass L, Matich G, Cringle SJ, Yu DY. Axonal transport and cytoskeletal changes in the laminar regions after elevated intraocular pressure. Invest Ophthalmol Vis Sci. 2007; 48:3632–3644. [PubMed: 17652733]

Baumann B, Rauscher S, Glosmann M, Gotzinger E, Pircher M, Fialova S, Groger M, Hitzenberger CK. Peripapillary rat sclera investigated in vivo with polarization-sensitive optical coherence tomography. Invest Ophthalmol Vis Sci. 2014; 55:7686–7696. [PubMed: 25352116]

Beirowski B, Nogradi A, Babetto E, Garcia-Alias G, Coleman MP. Mechanisms of axonal spheroid formation in central nervous system Wallerian degeneration. Journal of neuropathology and experimental neurology. 2010; 69:455–472. [PubMed: 20418780]

Boppart SA, Oldenburg AL, Xu C, Marks DL. Optical probes and techniques for molecular contrast enhancement in coherence imaging. J Biomed Opt. 2005; 10:41208. [PubMed: 16178632]

Bosco A, Romero CO, Breen KT, Chagovetz AA, Steele MR, Ambati BK, Vetter ML. Neurodegeneration severity is anticipated by early microglia alterations monitored in vivo in a mouse model of chronic glaucoma. Disease models & mechanisms. 2015

Braaf B, Vermeer KA, de Groot M, Vienola KV, de Boer JF. Fiber-based polarization-sensitive OCT of the human retina with correction of system polarization distortions. Biomed Opt Express. 2014; 5:2736–2758. [PubMed: 25136498]

Brown A. Axonal transport of membranous and nonmembranous cargoes: a unified perspective. J Cell Biol. 2003; 160:817–821. [PubMed: 12642609]

Bui BV, Batcha AH, Fletcher E, Wong VH, Fortune B. Relationship between the magnitude of intraocular pressure during an episode of acute elevation and retinal damage four weeks later in rats. PLoS One. 2013; 8:e70513. [PubMed: 23922999]

Bui BV, Edmunds B, Cioffi GA, Fortune B. The gradient of retinal functional changes during acute intraocular pressure elevation. Invest Ophthalmol Vis Sci. 2005; 46:202–213. [PubMed: 15623775]

Bui BV, Fortune B. Ganglion cell contributions to the rat full-field electroretinogram. J Physiol. 2004; 555:153–173. [PubMed: 14578484]

Burgoyne CF, Downs JC, Bellezza AJ, Suh JK, Hart RT. The optic nerve head as a biomechanical structure: a new paradigm for understanding the role of IOP-related stress and strain in the pathophysiology of glaucomatous optic nerve head damage. Prog Retin Eye Res. 2005; 24:39–73. [PubMed: 15555526]

Burgoyne CF, Quigley HA, Thompson HW, Vitale S, Varma R. Early changes in optic disc compliance and surface position in experimental glaucoma. Ophthalmology. 1995; 102:1800–1809. [PubMed: 9098280]

Burns SA, Tumbar R, Elsner AE, Ferguson D, Hammer DX. Large-field-of-view, modular, stabilized, adaptive-optics-based scanning laser ophthalmoscope. J Opt Soc Am A Opt Image Sci Vis. 2007; 24:1313–1326. [PubMed: 17429477]

Cense B, Chen TC, Park BH, Pierce MC, de Boer JF. Invivo depth-resolved birefringence measurements of the human retinal nerve fiber layer by polarization-sensitive optical coherence tomography. Opt Lett. 2002; 27:1610–1612. [PubMed: 18026517]

Cense B, Chen TC, Park BH, Pierce MC, de Boer JF. Thickness and birefringence of healthy retinal nerve fiber layer tissue measured with polarization-sensitive optical coherence tomography. Invest Ophthalmol Vis Sci. 2004; 45:2606–2612. [PubMed: 15277483]

Cense B, Gao W, Brown JM, Jones SM, Jonnal RS, Mujat M, Park BH, de Boer JF, Miller DT. Retinal imaging with polarization-sensitive optical coherence tomography and adaptive optics. Opt Express. 2009; 17:21634–21651. [PubMed: 19997405]

Cense B, Mujat M, Chen TC, Park BH, de Boer JF. Polarization-sensitive spectral-domain optical coherence tomography using a single line scan camera. Optics Express. 2007; 15:2421–2431. [PubMed: 19532479]

Chauhan BC, Burgoyne CF. From clinical examination of the optic disc to clinical assessment of the optic nerve head: a paradigm change. Am J Ophthalmol. 2013; 156:218–227. e212. [PubMed: 23768651]

Chauhan BC, O'Leary N, Almobarak FA, Reis AS, Yang H, Sharpe GP, Hutchison DM, Nicolela MT, Burgoyne CF. Enhanced detection of open-angle glaucoma with an anatomically accurate optical coherence tomography-derived neuroretinal rim parameter. Ophthalmology. 2013; 120:535–543. [PubMed: 23265804]

Chauhan BC, Pan J, Archibald ML, LeVatte TL, Kelly ME, Tremblay F. Effect of intraocular pressure on optic disc topography, electroretinography, and axonal loss in a chronic pressure-induced rat model of optic nerve damage. Invest Ophthalmol Vis Sci. 2002; 43:2969–2976. [PubMed: 12202517]

Chauhan BC, Stevens KT, Levesque JM, Nuschke AC, Sharpe GP, O'Leary N, Archibald ML, Wang X. Longitudinal in vivo imaging of retinal ganglion cells and retinal thickness changes following optic nerve injury in mice. PLoS One. 2012; 7:e40352. [PubMed: 22768284]

Chen MF, Chui TY, Alhadeff P, Rosen RB, Ritch R, Dubra A, Hood DC. Adaptive optics imaging of healthy and abnormal regions of retinal nerve fiber bundles of patients with glaucoma. Invest Ophthalmol Vis Sci. 2015; 56:674–681. [PubMed: 25574048]

Chen TC. Spectral domain optical coherence tomography in glaucoma: qualitative and quantitative analysis of the optic nerve head and retinal nerve fiber layer (an AOS thesis). Trans Am Ophthalmol Soc. 2009; 107:254–281. [PubMed: 20126502]

Chidlow G, Ebneter A, Wood JP, Casson RJ. The optic nerve head is the site of axonal transport disruption, axonal cytoskeleton damage and putative axonal regeneration failure in a rat model of glaucoma. Acta Neuropathol. 2011; 121:737–751. [PubMed: 21311901]

Choe TE, Abbott CJ, Piper C, Wang L, Fortune B. Comparison of longitudinal in vivo measurements of retinal nerve fiber layer thickness and retinal ganglion cell density after optic nerve transection in rat. PLoS One. 2014; 9:e113011. [PubMed: 25393294]

Chong RS, Martin KR. Retinal ganglion cell dendrites and glaucoma: a case of missing the wood for the trees? Expert Review of Ophthalmology. 2014; 9:149–152.

Cohan BE, Pearch AC, Jokelainen PT, Bohr DF. Optic disc imaging in conscious rats and mice. Invest Ophthalmol Vis Sci. 2003; 44:160–163. [PubMed: 12506069]

Coleman AL, Quigley HA, Vitale S, Dunkelberger G. Displacement of the optic nerve head by acute changes in intraocular pressure in monkey eyes. Ophthalmology. 1991; 98:35–40. [PubMed: 2023730]

Coleman M. Axon degeneration mechanisms: commonality amid diversity. Nat Rev Neurosci. 2005; 6:889–898. [PubMed: 16224497]

Cordeiro MF, Guo L, Luong V, Harding G, Wang W, Jones HE, Moss SE, Sillito AM, Fitzke FW. Real-time imaging of single nerve cell apoptosis in retinal neurodegeneration. Proc Natl Acad Sci U S A. 2004; 101:13352–13356. [PubMed: 15340151]

Costa RA, Skaf M, Melo LA Jr, Calucci D, Cardillo JA, Castro JC, Huang D, Wojtkowski M. Retinal assessment using optical coherence tomography. Prog Retin Eye Res. 2006; 25:325–353. [PubMed: 16716639]

Crish SD, Sappington RM, Inman DM, Horner PJ, Calkins DJ. Distal axonopathy with structural persistence in glaucomatous neurodegeneration. Proc Natl Acad Sci U S A. 2010; 107:5196–5201. [PubMed: 20194762]

Cull G, Burgoyne CF, Fortune B, Wang L. Longitudinal hemodynamic changes within the optic nerve head in experimental glaucoma. Invest Ophthalmol Vis Sci. 2013; 54:4271–4277. [PubMed: 23737471]

Cull GA, Reynaud J, Wang L, Cioffi GA, Burgoyne CF, Fortune B. Relationship between orbital optic nerve axon counts and retinal nerve fiber layer thickness measured by spectral domain optical coherence tomography. Invest Ophthalmol Vis Sci. 2012; 53:7766–7773. [PubMed: 23125332]

Cull GA, Reynaud J, Wang L, Cioffi GA, Burgoyne CF, Fortune B. Erratum in: “Relationship Between Orbital Optic Nerve Axon Counts and Retinal Nerve Fiber Layer Thickness Measured by Spectral Domain Optical Coherence Tomography”. Investigative Ophthalmology & Visual Science. 2014; 55:2619–2620.

Danesh-Meyer HV, Boland MV, Savino PJ, Miller NR, Subramanian PS, Girkin CA, Quigley HA. Optic Disc Morphology in Open Angle Glaucoma Compared with Anterior Ischemic Optic Neuropathies. Invest Ophthalmol Vis Sci. 2009

de la Zerda A, Prabhulkar S, Perez VL, Ruggeri M, Paranjape AS, Habte F, Gambhir SS, Awdeh RM. Optical coherence contrast imaging using gold nanorods in living mice eyes. Clin Experiment Ophthalmol. 2014

Drexler W, Fujimoto JG. State-of-the-art retinal optical coherence tomography. Prog Retin Eye Res. 2008; 27:45–88. [PubMed: 18036865]

Dwelle J, Liu S, Wang B, McElroy A, Ho D, Markey MK, Milner T, Rylander HG 3rd. Thickness, phase retardation, birefringence, and reflectance of the retinal nerve fiber layer in normal and

glaucomatous non-human primates. Invest Ophthalmol Vis Sci. 2012; 53:4380–4395. [PubMed: 22570345]

Elmaanaoui B, Wang B, Dwelle JC, McElroy AB, Liu SS, Rylander HG, Milner TE. Birefringence measurement of the retinal nerve fiber layer by swept source polarization sensitive optical coherence tomography. Opt Express. 2011; 19:10252–10268. [PubMed: 21643283]

Emery JM, Landis D, Paton D, Boniuk M, Craig JM. The lamina cribrosa in normal and glaucomatous human eyes. Transactions - American Academy of Ophthalmology and Otolaryngology. American Academy of Ophthalmology and Otolaryngology. 1974; 78:290–297.

Faridi OS, Park SC, Kabadi R, Su D, De Moraes CG, Liebmann JM, Ritch R. Effect of focal lamina cribrosa defect on glaucomatous visual field progression. Ophthalmology. 2014; 121:1524–1530. [PubMed: 24697910]

Felberer F, Kroisamer JS, Baumann B, Zotter S, Schmidt-Erfurth U, Hitzenberger CK, Pircher M. Adaptive optics SLO/OCT for 3D imaging of human photoreceptors in vivo. Biomed Opt Express. 2014; 5:439–456. [PubMed: 24575339]

Fingeret, M.; Flanagan, JG.; Liebmann, JM. The Essential HRT Primer. Jocoto Advertising, Inc; San Ramon, CA: 2005.

Fischer MD, Huber G, Beck SC, Tanimoto N, Muehlfriedel R, Fahl E, Grimm C, Wenzel A, Reme CE, van de Pavert SA, Wijnholds J, Pacal M, Bremner R, Seeliger MW. Noninvasive, in vivo assessment of mouse retinal structure using optical coherence tomography. PLoS One. 2009; 4:e7507. [PubMed: 19838301]

Fontana L, Bhandari A, Fitzke FW, Hitchings RA. In vivo morphometry of the lamina cribrosa and its relation to visual field loss in glaucoma. Curr Eye Res. 1998; 17:363–369. [PubMed: 9561827]

Fortune B, Bui BV, Morrison JC, Johnson EC, Dong J, Cepurna WO, Jia L, Barber S, Cioffi GA. Selective ganglion cell functional loss in rats with experimental glaucoma. Invest Ophthalmol Vis Sci. 2004; 45:1854–1862. [PubMed: 15161850]

Fortune B, Burgoyne CF, Cull G, Reynaud J, Wang L. Onset and progression of peripapillary retinal nerve fiber layer (RNFL) retardance changes occur earlier than RNFL thickness changes in experimental glaucoma. Invest Ophthalmol Vis Sci. 2013a; 54:5653–5661. [PubMed: 23847322]

Fortune B, Burgoyne CF, Cull GA, Reynaud J, Wang L. Structural and functional abnormalities of retinal ganglion cells measured in vivo at the onset of optic nerve head surface change in experimental glaucoma. Invest Ophthalmol Vis Sci. 2012; 53:3939–3950. [PubMed: 22589428]

Fortune B, Choe TE, Reynaud J, Hardin C, Cull GA, Burgoyne CF, Wang L. Deformation of the rodent optic nerve head and peripapillary structures during acute intraocular pressure elevation. Invest Ophthalmol Vis Sci. 2011; 52:6651–6661. [PubMed: 21730343]

Fortune B, Cull G, Reynaud J, Wang L, Burgoyne CF. Relating retinal ganglion cell function and retinal nerve fiber layer (RNFL) retardance to progressive loss of RNFL thickness and optic nerve axons in experimental glaucoma. Invest Ophthalmol Vis Sci. 2015; 56 in press.

Fortune B, Cull GA, Burgoyne CF. Relative course of retinal nerve fiber layer birefringence and thickness and retinal function changes after optic nerve transection. Invest Ophthalmol Vis Sci. 2008a; 49:4444–4452. [PubMed: 18566463]

Fortune B, Lusardi TA, Reynaud J, Choe TE, Piper C, Cull G, Burgoyne C, Wang L. Evidence of axonopathy during early-stage experimental glaucoma: relationship between in vivo imaging and histological findings. Invest Ophthalmol Vis Sci. 2014a; 55:E-Abstract 2644. manuscript in preparation.

Fortune B, Reynaud J, Cull G, Burgoyne CF, Wang L. The Effect of Age on Optic Nerve Axon Counts, SDOCT Scan Quality, and Peripapillary Retinal Nerve Fiber Layer Thickness Measurements in Rhesus Monkeys. Translational vision science & technology. 2014b; 3:2. [PubMed: 24932430]

Fortune B, Reynaud J, Wang L, Burgoyne CF. Does optic nerve head surface topography change prior to loss of retinal nerve fiber layer thickness: a test of the site of injury hypothesis in experimental glaucoma. PLoS One. 2013b; 8:e77831. [PubMed: 24204989]

Fortune B, Wang L, Cull G, Cioffi GA. Intravitreal colchicine causes decreased RNFL birefringence without altering RNFL thickness. Invest Ophthalmol Vis Sci. 2008b; 49:255–261. [PubMed: 18172100]

Fortune B, Yang H, Strouthidis NG, Cull GA, Grimm JL, Downs JC, Burgoyne CF. The effect of acute intraocular pressure elevation on peripapillary retinal thickness, retinal nerve fiber layer thickness, and retardance. Invest Ophthalmol Vis Sci. 2009; 50:4719–4726. [PubMed: 19420342]

Gabriele ML, Ishikawa H, Schuman JS, Ling Y, Bilonick RA, Kim JS, Kagemann L, Wollstein G. Optic nerve crush mice followed longitudinally with spectral domain optical coherence tomography. Invest Ophthalmol Vis Sci. 2011; 52:2250–2254. [PubMed: 21398282]

Gabriele Sandrian M, Wollstein G, Schuman JS, Bilonick RA, Ling Y, Ishikawa H, Kagemann L, McKenna KC. Inflammatory response to intravitreal injection of gold nanorods. Br J Ophthalmol. 2012; 96:1522–1529. [PubMed: 23087415]

Gardiner SK, Ren R, Yang H, Fortune B, Burgoyne CF, Demirel S. A method to estimate the amount of neuroretinal rim tissue in glaucoma: comparison with current methods for measuring rim area. Am J Ophthalmol. 2014; 157:540–549. e541–542. [PubMed: 24239775]

Geng Y, Dubra A, Yin L, Merigan WH, Sharma R, Libby RT, Williams DR. Adaptive optics retinal imaging in the living mouse eye. Biomed Opt Express. 2012; 3:715–734. [PubMed: 22574260]

Geng Y, Greenberg KP, Wolfe R, Gray DC, Hunter JJ, Dubra A, Flannery JG, Williams DR, Porter J. In vivo imaging of microscopic structures in the rat retina. Invest Ophthalmol Vis Sci. 2009; 50:5872–5879. [PubMed: 19578019]

Girard MJ, Tun TA, Husain R, Acharyya S, Haaland BA, Wei X, Mari JM, Perera SA, Baskaran M, Aung T, Strouthidis NG. Lamina cribrosa visibility using optical coherence tomography: comparison of devices and effects of image enhancement techniques. Invest Ophthalmol Vis Sci. 2015; 56:865–874. [PubMed: 25593025]

Goldblum D, Mittag T. Prospects for relevant glaucoma models with retinal ganglion cell damage in the rodent eye. Vision Res. 2002; 42:471–478. [PubMed: 11853763]

Gordon AY, Jayagopal A. Engineering of Nanoscale Contrast Agents for Optical Coherence Tomography. Journal of nanomedicine & nanotechnology. 2014; (Suppl 5):004. [PubMed: 25009761]

Gotzinger E, Pircher M, Hitzenberger CK. High speed spectral domain polarization sensitive optical coherence tomography of the human retina. Opt Express. 2005; 13:10217–10229. [PubMed: 19503236]

Gramlich OW, Lueckner TC, Kriechbaum M, Teister J, Tao X, von Pein HD, Pfeiffer N, Grus FH. Dynamics, alterations, and consequences of minimally invasive intraocular pressure elevation in rats. Invest Ophthalmol Vis Sci. 2014; 55:600–611. [PubMed: 24408983]

Gray DC, Wolfe R, Gee BP, Scoles D, Geng Y, Masella BD, Dubra A, Luque S, Williams DR, Merigan WH. In vivo imaging of the fine structure of rhodamine-labeled macaque retinal ganglion cells. Invest Ophthalmol Vis Sci. 2008; 49:467–473. [PubMed: 18172127]

Greaney MJ, Hoffman DC, Garway-Heath DF, Nakla M, Coleman AL, Caprioli J. Comparison of optic nerve imaging methods to distinguish normal eyes from those with glaucoma. Invest Ophthalmol Vis Sci. 2002; 43:140–145. [PubMed: 11773024]

Greenfield DS, Bagga H, Knighton RW. Macular thickness changes in glaucomatous optic neuropathy detected using optical coherence tomography. Arch Ophthalmol. 2003; 121:41–46. [PubMed: 12523883]

Guo L, Normando EM, Nizari S, Lara D, Cordeiro MF. Tracking longitudinal retinal changes in experimental ocular hypertension using the cSLO and spectral domain-OCT. Invest Ophthalmol Vis Sci. 2010; 51:6504–6513. [PubMed: 20688741]

Guo L, Tsatourian V, Luong V, Podoleanu AG, Jackson DA, Fitzke FW, Cordeiro MF. En face optical coherence tomography: a new method to analyse structural changes of the optic nerve head in rat glaucoma. Br J Ophthalmol. 2005; 89:1210–1216. [PubMed: 16113384]

Hare WA, WoldeMussie E, Weinreb RN, Ton H, Ruiz G, Wijono M, Feldmann B, Zangwill L, Wheeler L. Efficacy and safety of memantine treatment for reduction of changes associated with experimental glaucoma in monkey, II: Structural measures. Invest Ophthalmol Vis Sci. 2004; 45:2640–2651. [PubMed: 15277487]

Hawes NL, Smith RS, Chang B, Davisson M, Heckenlively JR, John SW. Mouse fundus photography and angiography: a catalogue of normal and mutant phenotypes. Mol Vis. 1999; 5:22. [PubMed: 10493779]

He L, Yang H, Gardiner SK, Williams G, Hardin C, Strouthidis NG, Fortune B, Burgoyne CF. Longitudinal detection of optic nerve head changes by spectral domain optical coherence tomography in early experimental glaucoma. Invest Ophthalmol Vis Sci. 2014; 55:574–586. [PubMed: 24255047]

Heickell AG, Bellezza AJ, Thompson HW, Burgoyne CF. Optic disc surface compliance testing using confocal scanning laser tomography in the normal monkey eye. J Glaucoma. 2001; 10:369–382. [PubMed: 11711833]

Hermann B, Fernandez EJ, Unterhuber A, Sattmann H, Fercher AF, Drexler W, Prieto PM, Artal P. Adaptive-optics ultrahigh-resolution optical coherence tomography. Opt Lett. 2004; 29:2142–2144. [PubMed: 15460883]

Higashide T, Kawaguchi I, Ohkubo S, Takeda H, Sugiyama K. In vivo imaging and counting of rat retinal ganglion cells using a scanning laser ophthalmoscope. Invest Ophthalmol Vis Sci. 2006; 47:2943–2950. [PubMed: 16799037]

Ho G, Kumar S, Min XS, Kng YL, Loh MY, Gao S, Zhuo L. Molecular imaging of retinal gliosis in transgenic mice induced by kainic acid neurotoxicity. Invest Ophthalmol Vis Sci. 2009; 50:2459–2464. [PubMed: 19151398]

Hong YJ, Miura M, Ju MJ, Makita S, Iwasaki T, Yasuno Y. Simultaneous investigation of vascular and retinal pigment epithelial pathologies of exudative macular diseases by multifunctional optical coherence tomography. Invest Ophthalmol Vis Sci. 2014; 55:5016–5031. [PubMed: 25052993]

Hood DC, Raza AS, de Moraes CG, Liebmann JM, Ritch R. Glaucomatous damage of the macula. Prog Retin Eye Res. 2013; 32:1–21. [PubMed: 22995953]

Hood DC, Slobodnick A, Raza AS, de Moraes CG, Teng CC, Ritch R. Early glaucoma involves both deep local, and shallow widespread, retinal nerve fiber damage of the macular region. Invest Ophthalmol Vis Sci. 2014; 55:632–649. [PubMed: 24370831]

Howell GR, Libby RT, Jakobs TC, Smith RS, Phalan FC, Barter JW, Barbay JM, Marchant JK, Mahesh N, Porciatti V, Whitmore AV, Masland RH, John SW. Axons of retinal ganglion cells are insulted in the optic nerve early in DBA/2J glaucoma. J Cell Biol. 2007; 179:1523–1537. [PubMed: 18158332]

Howell GR, Soto I, Libby RT, John SW. Intrinsic axonal degeneration pathways are critical for glaucomatous damage. Exp Neurol. 2012

Hoyt WF, Frisen L, Newman NM. Fundoscopy of nerve fiber layer defects in glaucoma. Invest Ophthalmol. 1973; 12:814–829. [PubMed: 4752920]

Hoyt WF, Newman NM. The earliest observable defect in glaucoma? Lancet. 1972; 1:692–693. [PubMed: 4125199]

Huang D, Swanson EA, Lin CP, Schuman JS, Stinson WG, Chang W, Hee MR, Flotte T, Gregory K, Puliafito CA, et al. Optical coherence tomography. Science. 1991; 254:1178–1181. [PubMed: 1957169]

Huang G, Gast TJ, Burns SA. In vivo adaptive optics imaging of the temporal raphe and its relationship to the optic disc and fovea in the human retina. Invest Ophthalmol Vis Sci. 2014; 55:5952–5961. [PubMed: 25146991]

Huang X, Kong W, Zhou Y, Gregori G. Distortion of axonal cytoskeleton: an early sign of glaucomatous damage. Invest Ophthalmol Vis Sci. 2011a; 52:2879–2888. [PubMed: 21245391]

Huang XR, Bagga H, Greenfield DS, Knighton RW. Variation of peripapillary retinal nerve fiber layer birefringence in normal human subjects. Invest Ophthalmol Vis Sci. 2004; 45:3073–3080. [PubMed: 15326123]

Huang XR, Knighton RW. Linear birefringence of the retinal nerve fiber layer measured in vitro with a multispectral imaging micropolarimeter. J Biomed Opt. 2002; 7:199–204. [PubMed: 11966304]

Huang XR, Knighton RW. Microtubules contribute to the birefringence of the retinal nerve fiber layer. Invest Ophthalmol Vis Sci. 2005; 46:4588–4593. [PubMed: 16303953]

Huang XR, Knighton RW. Altered F-actin distribution in retinal nerve fiber layer of a rat model of glaucoma. Exp Eye Res. 2009; 88:1107–1114. [PubMed: 19450448]

Huang XR, Knighton RW, Cavuoto LN. Microtubule contribution to the reflectance of the retinal nerve fiber layer. Invest Ophthalmol Vis Sci. 2006; 47:5363–5367. [PubMed: 17122125]

Huang XR, Knighton RW, Zhou Y, Zhao XP. Reflectance speckle of retinal nerve fiber layer reveals axonal activity. Invest Ophthalmol Vis Sci. 2013; 54:2616–2623. [PubMed: 23532525]

Huang XR, Zhou Y, Kong W, Knighton RW. Reflectance decreases before thickness changes in the retinal nerve fiber layer in glaucomatous retinas. Invest Ophthalmol Vis Sci. 2011b; 52:6737–6742. [PubMed: 21730345]

Inoue R, Hangai M, Kotera Y, Nakanishi H, Mori S, Morishita S, Yoshimura N. Three-dimensional high-speed optical coherence tomography imaging of lamina cribrosa in glaucoma. Ophthalmology. 2009; 116:214–222. [PubMed: 19091413]

Ishikawa H, Stein DM, Wollstein G, Beaton S, Fujimoto JG, Schuman JS. Macular segmentation with optical coherence tomography. Invest Ophthalmol Vis Sci. 2005; 46:2012–2017. [PubMed: 15914617]

Ivers KM, Li C, Patel N, Sredar N, Luo X, Queener H, Harwerth RS, Porter J. Reproducibility of measuring lamina cribrosa pore geometry in human and nonhuman primates with in vivo adaptive optics imaging. Invest Ophthalmol Vis Sci. 2011; 52:5473–5480. [PubMed: 21546533]

Jakobs TC, Libby RT, Ben Y, John SW, Masland RH. Retinal ganglion cell degeneration is topological but not cell type specific in DBA/2J mice. J Cell Biol. 2005; 171:313–325. [PubMed: 16247030]

Jian Y, Zawadzki RJ, Sarunic MV. Adaptive optics optical coherence tomography for in vivo mouse retinal imaging. J Biomed Opt. 2013; 18:56007. [PubMed: 23644903]

Jung Y, Reif R, Zeng Y, Wang RK. Three-dimensional high-resolution imaging of gold nanorods uptake in sentinel lymph nodes. Nano Lett. 2011; 11:2938–2943. [PubMed: 21667930]

Kagemann L, Ishikawa H, Wollstein G, Brennen PM, Townsend KA, Gabriele ML, Schuman JS. Ultrahigh-resolution spectral domain optical coherence tomography imaging of the lamina cribrosa. Ophthalmic Surg Lasers Imaging. 2008; 39:S126–131. [PubMed: 18777881]

Kamal DS, Garway-Heath DF, Hitchings RA, Fitzke FW. Use of sequential Heidelberg retina tomograph images to identify changes at the optic disc in ocular hypertensive patients at risk of developing glaucoma. Br J Ophthalmol. 2000; 84:993–998. [PubMed: 10966952]

Kanamori A, Catrinescu MM, Belisle JM, Costantino S, Levin LA. Retrograde and Wallerian axonal degeneration occur synchronously after retinal ganglion cell axotomy. Am J Pathol. 2012; 181:62–73. [PubMed: 22642911]

Kanamori A, Catrinescu MM, Traistaru M, Beaubien R, Levin LA. In vivo imaging of retinal ganglion cell axons within the nerve fiber layer. Invest Ophthalmol Vis Sci. 2010; 51:2011–2018. [PubMed: 19797216]

Kashiwagi K, Ou B, Nakamura S, Tanaka Y, Suzuki M, Tsukahara S. Increase in dephosphorylation of the heavy neurofilament subunit in the monkey chronic glaucoma model. Invest Ophthalmol Vis Sci. 2003; 44:154–159. [PubMed: 12506068]

Kawaguchi I, Higashide T, Ohkubo S, Takeda H, Sugiyama K. In vivo imaging and quantitative evaluation of the rat retinal nerve fiber layer using scanning laser ophthalmoscopy. Invest Ophthalmol Vis Sci. 2006; 47:2911–2916. [PubMed: 16799033]

Kim DY, Werner JS, Zawadzki RJ. Complex conjugate artifact-free adaptive optics optical coherence tomography of in vivo human optic nerve head. J Biomed Opt. 2012; 17:126005. [PubMed: 23208216]

Klein T, Wieser W, Reznicek L, Neubauer A, Kampik A, Huber R. Multi-MHz retinal OCT. Biomed Opt Express. 2013; 4:1890–1908. [PubMed: 24156052]

Knighton RW, Huang X, Zhou Q. Microtubule contribution to the reflectance of the retinal nerve fiber layer. Invest Ophthalmol Vis Sci. 1998; 39:189–193. [PubMed: 9430561]

Knighton RW, Huang XR. Directional and spectral reflectance of the rat retinal nerve fiber layer. Invest Ophthalmol Vis Sci. 1999; 40:639–647. [PubMed: 10067967]

Knighton RW, Jacobson SG, Kemp CM. The spectral reflectance of the nerve fiber layer of the macaque retina. Invest Ophthalmol Vis Sci. 1989; 30:2392–2402. [PubMed: 2807795]

Knighton RW, Qian C. An optical model of the human retinal nerve fiber layer: implications of directional reflectance for variability of clinical measurements. J Glaucoma. 2000; 9:56–62. [PubMed: 10708233]

Knighton RW, Zhou Q. The relation between the reflectance and thickness of the retinal nerve fiber layer. J Glaucoma. 1995; 4:117–123. [PubMed: 19920656]

Kocaoglu OP, Cense B, Jonnal RS, Wang Q, Lee S, Gao W, Miller DT. Imaging retinal nerve fiber bundles using optical coherence tomography with adaptive optics. Vision Res. 2011; 51:1835–1844. [PubMed: 21722662]

Kocaoglu OP, Ferguson RD, Jonnal RS, Liu Z, Wang Q, Hammer DX, Miller DT. Adaptive optics optical coherence tomography with dynamic retinal tracking. Biomed Opt Express. 2014a; 5:2262–2284. [PubMed: 25071963]

Kocaoglu OP, Turner TL, Liu Z, Miller DT. Adaptive optics optical coherence tomography at 1 MHz. Biomed Opt Express. 2014b; 5:4186–4200. [PubMed: 25574431]

Kocaoglu OP, Uhlhorn SR, Hernandez E, Juarez RA, Will R, Parel JM, Manns F. Simultaneous fundus imaging and optical coherence tomography of the mouse retina. Invest Ophthalmol Vis Sci. 2007; 48:1283–1289. [PubMed: 17325174]

Lalezary M, Medeiros FA, Weinreb RN, Bowd C, Sample PA, Tavares IM, Tafreshi A, Zangwill LM. Baseline optical coherence tomography predicts the development of glaucomatous change in glaucoma suspects. Am J Ophthalmol. 2006; 142:576–582. [PubMed: 17011848]

Lee EJ, Kim TW, Weinreb RN, Suh MH, Kang M, Park KH, Kim SH, Kim DM. Three-dimensional evaluation of the lamina cribrosa using spectral-domain optical coherence tomography in glaucoma. Invest Ophthalmol Vis Sci. 2012; 53:198–204. [PubMed: 22167102]

Lemij HG, Reus NJ. New developments in scanning laser polarimetry for glaucoma. Curr Opin Ophthalmol. 2008; 19:136–140. [PubMed: 18301287]

Leung CK. Diagnosing glaucoma progression with optical coherence tomography. Curr Opin Ophthalmol. 2014; 25:104–111. [PubMed: 24370973]

Leung CK, Lindsey JD, Crowston JG, Ju WK, Liu Q, Bartsch DU, Weinreb RN. In vivo imaging of murine retinal ganglion cells. J Neurosci Methods. 2008a; 168:475–478. [PubMed: 18079000]

Leung CK, Lindsey JD, Crowston JG, Lijia C, Chiang S, Weinreb RN. Longitudinal profile of retinal ganglion cell damage after optic nerve crush with blue-light confocal scanning laser ophthalmoscopy. Invest Ophthalmol Vis Sci. 2008b; 49:4898–4902. [PubMed: 18441315]

Leung CK, Weinreb RN, Li ZW, Liu S, Lindsey JD, Choi N, Liu L, Cheung CY, Ye C, Qiu K, Chen LJ, Yung WH, Crowston JG, Pu M, So KF, Pang CP, Lam DS. Long-term in vivo imaging and measurement of dendritic shrinkage of retinal ganglion cells. Invest Ophthalmol Vis Sci. 2011; 52:1539–1547. [PubMed: 21245394]

Li ZW, Liu S, Weinreb RN, Lindsey JD, Yu M, Liu L, Ye C, Cui Q, Yung WH, Pang CP, Lam DS, Leung CK. Tracking dendritic shrinkage of retinal ganglion cells after acute elevation of intraocular pressure. Invest Ophthalmol Vis Sci. 2011; 52:7205–7212. [PubMed: 21775662]

Liang J, Williams DR, Miller DT. Supernormal vision and high-resolution retinal imaging through adaptive optics. J Opt Soc Am A Opt Image Sci Vis. 1997; 14:2884–2892. [PubMed: 9379246]

Lisboa R, Paranhos A Jr, Weinreb RN, Zangwill LM, Leite MT, Medeiros FA. Comparison of different spectral domain OCT scanning protocols for diagnosing preperimetric glaucoma. Invest Ophthalmol Vis Sci. 2013; 54:3417–3425. [PubMed: 23532529]

Liu Y, McDowell CM, Zhang Z, Tebow HE, Wordinger RJ, Clark AF. Monitoring retinal morphologic and functional changes in mice following optic nerve crush. Invest Ophthalmol Vis Sci. 2014; 55:3766–3774. [PubMed: 24854856]

Lozano DC, Twa MD. Development of a rat schematic eye from in vivo biometry and the correction of lateral magnification in SD-OCT imaging. Invest Ophthalmol Vis Sci. 2013; 54:6446–6455. [PubMed: 23989191]

Luo X, Patel NB, Rajagopalan LP, Harwerth RS, Frishman LJ. Relation between macular retinal ganglion cell/inner plexiform layer thickness and multifocal electroretinogram measures in experimental glaucoma. Invest Ophthalmol Vis Sci. 2014; 55:4512–4524. [PubMed: 24970256]

Lye-Barthel M, Sun D, Jakobs TC. Morphology of astrocytes in a glaucomatous optic nerve. Invest Ophthalmol Vis Sci. 2013; 54:909–917. [PubMed: 23322566]

Mari JM, Strouthidis NG, Park SC, Girard MJ. Enhancement of lamina cribrosa visibility in optical coherence tomography images using adaptive compensation. Invest Ophthalmol Vis Sci. 2013; 54:2238–2247. [PubMed: 23449723]

Martin KR, Quigley HA, Valenta D, Kielczewski J, Pease ME. Optic nerve dynein motor protein distribution changes with intraocular pressure elevation in a rat model of glaucoma. Exp Eye Res. 2006; 83:255–262. [PubMed: 16546168]

May CA, Lutjen-Drecoll E. Morphology of the murine optic nerve. Invest Ophthalmol Vis Sci. 2002; 43:2206–2212. [PubMed: 12091418]

Medeiros FA, Bowd C, Zangwill LM, Patel C, Weinreb RN. Detection of glaucoma using scanning laser polarimetry with enhanced corneal compensation. Invest Ophthalmol Vis Sci. 2007; 48:3146–3153. [PubMed: 17591884]

Medeiros FA, Zangwill LM, Bowd C, Mohammadi K, Weinreb RN. Comparison of scanning laser polarimetry using variable corneal compensation and retinal nerve fiber layer photography for detection of glaucoma. Arch Ophthalmol. 2004; 122:698–704. [PubMed: 15136317]

Mohammadi K, Bowd C, Weinreb RN, Medeiros FA, Sample PA, Zangwill LM. Retinal nerve fiber layer thickness measurements with scanning laser polarimetry predict glaucomatous visual field loss. Am J Ophthalmol. 2004; 138:592–601. [PubMed: 15488786]

Moreno PA, Konno B, Lima VC, Castro DP, Castro LC, Leite MT, Pacheco MA, Lee JM, Prata TS. Spectral-domain optical coherence tomography for early glaucoma assessment: analysis of macular ganglion cell complex versus peripapillary retinal nerve fiber layer. Can J Ophthalmol. 2011; 46:543–547. [PubMed: 22153644]

Morgan JE. Retina ganglion cell degeneration in glaucoma: an opportunity missed? A review. Clin Experiment Ophthalmol. 2012; 40:364–368. [PubMed: 22404820]

Morrison J, Farrell S, Johnson E, Deppmeier L, Moore CG, Grossmann E. Structure and composition of the rodent lamina cribrosa. Exp Eye Res. 1995; 60:127–135. [PubMed: 7781741]

Morrison JC, Johnson E, Cepurna WO. Rat models for glaucoma research. Prog Brain Res. 2008; 173:285–301. [PubMed: 18929117]

Morrison JC, Moore CG, Deppmeier LM, Gold BG, Meshul CK, Johnson EC. A rat model of chronic pressure-induced optic nerve damage. Exp Eye Res. 1997; 64:85–96. [PubMed: 9093024]

Murata H, Aihara M, Chen YN, Ota T, Numaga J, Araie M. Imaging mouse retinal ganglion cells and their loss in vivo by a fundus camera in the normal and ischemia-reperfusion model. Invest Ophthalmol Vis Sci. 2008; 49:5546–5552. [PubMed: 18689704]

Nadler Z, Wang B, Schuman JS, Ferguson RD, Patel A, Hammer DX, Bilonick RA, Ishikawa H, Kagemann L, Sigal IA, Wollstein G. In vivo three-dimensional characterization of the healthy human lamina cribrosa with adaptive optics spectral-domain optical coherence tomography. Invest Ophthalmol Vis Sci. 2014a; 55:6459–6466. [PubMed: 25228539]

Nadler Z, Wang B, Wollstein G, Nevins JE, Ishikawa H, Bilonick R, Kagemann L, Sigal IA, Ferguson RD, Patel A, Hammer DX, Schuman JS. Repeatability of in vivo 3D lamina cribrosa microarchitecture using adaptive optics spectral domain optical coherence tomography. Biomed Opt Express. 2014b; 5:1114–1123. [PubMed: 24761293]

Nagata A, Higashide T, Ohkubo S, Takeda H, Sugiyama K. In vivo quantitative evaluation of the rat retinal nerve fiber layer with optical coherence tomography. Invest Ophthalmol Vis Sci. 2009; 50:2809–2815. [PubMed: 19182247]

Nakano N, Ikeda HO, Hangai M, Muraoka Y, Toda Y, Kakizuka A, Yoshimura N. Longitudinal and simultaneous imaging of retinal ganglion cells and inner retinal layers in a mouse model of glaucoma induced by N-methyl-D-aspartate. Invest Ophthalmol Vis Sci. 2011; 52:8754–8762. [PubMed: 22003119]

Naskar R, Wissing M, Thanos S. Detection of early neuron degeneration and accompanying microglial responses in the retina of a rat model of glaucoma. Invest Ophthalmol Vis Sci. 2002; 43:2962–2968. [PubMed: 12202516]

Nickells RW, Howell GR, Soto I, John SW. Under pressure: cellular and molecular responses during glaucoma, a common neurodegeneration with axonopathy. Annu Rev Neurosci. 2012; 35:153–179. [PubMed: 22524788]

O'Leary N, Crabb DP, Mansberger SL, Fortune B, Twa MD, Lloyd MJ, Kotecha A, Garway-Heath DF, Cioffi GA, Johnson CA. Glaucomatous progression in series of stereoscopic photographs and Heidelberg retina tomograph images. Arch Ophthalmol. 2010; 128:560–568. [PubMed: 20457976]

Pang IH, Clark AF. Rodent models for glaucoma retinopathy and optic neuropathy. J Glaucoma. 2007; 16:483–505. [PubMed: 17700292]

Paques M, Guyomard JL, Simonutti M, Roux MJ, Picaud S, Legargasson JF, Sahel JA. Panretinal, high-resolution color photography of the mouse fundus. Invest Ophthalmol Vis Sci. 2007; 48:2769–2774. [PubMed: 17525211]

Paques M, Simonutti M, Roux MJ, Picaud S, Levavasseur E, Bellman C, Sahel JA. High resolution fundus imaging by confocal scanning laser ophthalmoscopy in the mouse. Vision Res. 2006; 46:1336–1345. [PubMed: 16289196]

Park HY, Jeon SH, Park CK. Enhanced depth imaging detects lamina cribrosa thickness differences in normal tension glaucoma and primary open-angle glaucoma. Ophthalmology. 2012a; 119:10–20. [PubMed: 22015382]

Park SC, De Moraes CG, Teng CC, Tello C, Liebmann JM, Ritch R. Enhanced depth imaging optical coherence tomography of deep optic nerve complex structures in glaucoma. Ophthalmology. 2012b; 119:3–9. [PubMed: 21978593]

Patel NB, Sullivan-Mee M, Harwerth RS. The relationship between retinal nerve fiber layer thickness and optic nerve head neuroretinal rim tissue in glaucoma. Invest Ophthalmol Vis Sci. 2014; 55:6802–6816. [PubMed: 25249610]

Pircher M, Hitzenberger CK, Schmidt-Erfurth U. Polarization sensitive optical coherence tomography in the human eye. Prog Retin Eye Res. 2011; 30:431–451. [PubMed: 21729763]

Pocock GM, Aranibar RG, Kemp NJ, Specht CS, Markey MK, Rylander HG 3rd. The relationship between retinal ganglion cell axon constituents and retinal nerve fiber layer birefringence in the primate. Invest Ophthalmol Vis Sci. 2009; 50:5238–5246. [PubMed: 19494208]

Povazay B, Hofer B, Hermann B, Unterhuber A, Morgan JE, Glittenberg C, Binder S, Drexler W. Minimum distance mapping using three-dimensional optical coherence tomography for glaucoma diagnosis. J Biomed Opt. 2007; 12:041204. [PubMed: 17867793]

Prilloff S, Fan J, Henrich-Noack P, Sabel BA. In vivo confocal neuroimaging (ICON): non-invasive, functional imaging of the mammalian CNS with cellular resolution. Eur J Neurosci. 2010; 31:521–528. [PubMed: 20105236]

Quigley HA. Examination of the retinal nerve fiber layer in the recognition of early glaucoma damage. Trans Am Ophthalmol Soc. 1986; 84:920–966. [PubMed: 3109098]

Quigley HA. Open-angle glaucoma. N Engl J Med. 1993; 328:1097–1106. [PubMed: 8455668]

Quigley HA. Neuronal death in glaucoma. Prog Retin Eye Res. 1999; 18:39–57. [PubMed: 9920498]

Quigley HA. Glaucoma. Lancet. 2011; 377:1367–1377. [PubMed: 21453963]

Quigley HA, Addicks EM. Quantitative studies of retinal nerve fiber layer defects. Arch Ophthalmol. 1982; 100:807–814. [PubMed: 7082210]

Quigley HA, Addicks EM, Green WR, Maumenee AE. Optic nerve damage in human glaucoma. II. The site of injury and susceptibility to damage. Arch Ophthalmol. 1981; 99:635–649. [PubMed: 6164357]

Quigley HA, Broman AT. The number of people with glaucoma worldwide in 2010 and 2020. Br J Ophthalmol. 2006; 90:262–267. [PubMed: 16488940]

Raff MC, Whitmore AV, Finn JT. Axonal self-destruction and neurodegeneration. Science. 2002; 296:868–871. [PubMed: 11988563]

Rao HL, Addepalli UK, Chaudhary S, Kumbar T, Senthil S, Choudhari NS, Garudadri CS. Ability of different scanning protocols of spectral domain optical coherence tomography to diagnose preperimetric glaucoma. Invest Ophthalmol Vis Sci. 2013; 54:7252–7257. [PubMed: 24114539]

Raza AS, Cho J, de Moraes CG, Wang M, Zhang X, Kardon RH, Liebmann JM, Ritch R, Hood DC. Retinal ganglion cell layer thickness and local visual field sensitivity in glaucoma. Arch Ophthalmol. 2011; 129:1529–1536. [PubMed: 22159673]

Reus NJ, Lemij HG. Diagnostic accuracy of the GDx VCC for glaucoma. Ophthalmology. 2004; 111:1860–1865. [PubMed: 15465547]

Roorda A, Romero-Borja F, Donnelly W III, Queener H, Hebert T, Campbell M. Adaptive optics scanning laser ophthalmoscopy. Opt Express. 2002; 10:405–412. [PubMed: 19436374]

Ruggeri M, Wehbe H, Jiao S, Gregori G, Jockovich ME, Hackam A, Duan Y, Puliafito CA. In vivo three-dimensional high-resolution imaging of rodent retina with spectral-domain optical coherence tomography. Invest Ophthalmol Vis Sci. 2007; 48:1808–1814. [PubMed: 17389515]

Rylander HG 3rd, Kemp NJ, Park J, Zaatari HN, Milner TE. Birefringence of the primate retinal nerve fiber layer. Exp Eye Res. 2005; 81:81–89. [PubMed: 15978258]

Sabel BA, Engelmann R, Humphrey MF. In vivo confocal neuroimaging (ICON) of CNS neurons. Nat Med. 1997; 3:244–247. [PubMed: 9018248]

Sakamoto A, Hangai M, Nukada M, Nakanishi H, Mori S, Kotera Y, Inoue R, Yoshimura N. Three-dimensional imaging of the macular retinal nerve fiber layer in glaucoma with spectral-domain optical coherence tomography. Invest Ophthalmol Vis Sci. 2010; 51:5062–5070. [PubMed: 20463326]

Salinas-Navarro M, Alarcon-Martinez L, Valiente-Soriano FJ, Jimenez-Lopez M, Mayor-Torroglosa S, Aviles-Trigueros M, Villegas-Perez MP, Vidal-Sanz M. Ocular hypertension impairs optic nerve axonal transport leading to progressive retinal ganglion cell degeneration. Exp Eye Res. 2010; 90:168–183. [PubMed: 19835874]

Schlamp CL, Li Y, Dietz JA, Janssen KT, Nickells RW. Progressive ganglion cell loss and optic nerve degeneration in DBA/2J mice is variable and asymmetric. BMC Neurosci. 2006; 7:66. [PubMed: 17018142]

Schuman JS, Hee MR, Puliafito CA, Wong C, Pedut-Kloizman T, Lin CP, Hertzmark E, Izatt JA, Swanson EA, Fujimoto JG. Quantification of nerve fiber layer thickness in normal and glaucomatous eyes using optical coherence tomography. Arch Ophthalmol. 1995; 113:586–596. [PubMed: 7748128]

Schuman JS, Pedut-Kloizman T, Pakter H, Wang N, Guedes V, Huang L, Pieroth L, Scott W, Hee MR, Fujimoto JG, Ishikawa H, Bilonick RA, Kagemann L, Wollstein G. Optical coherence tomography and histologic measurements of nerve fiber layer thickness in normal and glaucomatous monkey eyes. Invest Ophthalmol Vis Sci. 2007; 48:3645–3654. [PubMed: 17652734]

Seeliger MW, Beck SC, Pereyra-Munoz N, Dangel S, Tsai JY, Luhmann UF, van de Pavert SA, Wijnholds J, Samardzija M, Wenzel A, Zrenner E, Narfstrom K, Fahl E, Tanimoto N, Acar N, Tonagel F. In vivo confocal imaging of the retina in animal models using scanning laser ophthalmoscopy. Vision Res. 2005; 45:3512–3519. [PubMed: 16188288]

Sharma P, Sample PA, Zangwill LM, Schuman JS. Diagnostic tools for glaucoma detection and management. Surv Ophthalmol. 2008; 53(Suppl 1):S17–32. [PubMed: 19038620]

Shimazawa M, Tomita G, Taniguchi T, Sasaoka M, Hara H, Kitazawa Y, Araie M. Morphometric evaluation of changes with time in optic disc structure and thickness of retinal nerve fibre layer in chronic ocular hypertensive monkeys. Exp Eye Res. 2006; 82:427–440. [PubMed: 16388801]

Shou T, Liu J, Wang W, Zhou Y, Zhao K. Differential dendritic shrinkage of alpha and beta retinal ganglion cells in cats with chronic glaucoma. Invest Ophthalmol Vis Sci. 2003; 44:3005–3010. [PubMed: 12824245]

Sommer A, Katz J, Quigley HA, Miller NR, Robin AL, Richter RC, Witt KA. Clinically detectable nerve fiber atrophy precedes the onset of glaucomatous field loss. Arch Ophthalmol. 1991; 109:77–83. [PubMed: 1987954]

Soto I, Oglesby E, Buckingham BP, Son JL, Roberson ED, Steele MR, Inman DM, Vetter ML, Horner PJ, Marsh-Armstrong N. Retinal ganglion cells downregulate gene expression and lose their axons within the optic nerve head in a mouse glaucoma model. J Neurosci. 2008; 28:548–561. [PubMed: 18184797]

Soto I, Pease ME, Son JL, Shi X, Quigley HA, Marsh-Armstrong N. Retinal ganglion cell loss in a rat ocular hypertension model is sectorial and involves early optic nerve axon loss. Invest Ophthalmol Vis Sci. 2011; 52:434–441. [PubMed: 20811062]

Sredar N, Ivers KM, Queener HM, Zouridakis G, Porter J. 3D modeling to characterize lamina cribrosa surface and pore geometries using in vivo images from normal and glaucomatous eyes. Biomed Opt Express. 2013; 4:1153–1165. [PubMed: 23847739]

Srinivasan PP, Heflin SJ, Izatt JA, Arshavsky VY, Farsiu S. Automatic segmentation of up to ten layer boundaries in SD-OCT images of the mouse retina with and without missing layers due to pathology. Biomed Opt Express. 2014; 5:348–365. [PubMed: 24575332]

Srinivasan VJ, Adler DC, Chen Y, Gorczynska I, Huber R, Duker JS, Schuman JS, Fujimoto JG. Ultrahigh-speed optical coherence tomography for three-dimensional and en face imaging of the retina and optic nerve head. Invest Ophthalmol Vis Sci. 2008; 49:5103–5110. [PubMed: 18658089]

Srinivasan VJ, Ko TH, Wojtkowski M, Carvalho M, Clermont A, Bursell SE, Song QH, Lem J, Duker JS, Schuman JS, Fujimoto JG. Noninvasive volumetric imaging and morphometry of the rodent retina with high-speed, ultrahigh-resolution optical coherence tomography. Invest Ophthalmol Vis Sci. 2006; 47:5522–5528. [PubMed: 17122144]

Strouthidis NG, Fortune B, Yang H, Sigal IA, Burgoyne CF. Effect of acute intraocular pressure elevation on the monkey optic nerve head as detected by spectral domain optical coherence tomography. Invest Ophthalmol Vis Sci. 2011a; 52:9431–9437. [PubMed: 22058335]

Strouthidis NG, Fortune B, Yang H, Sigal IA, Burgoyne CF. Longitudinal change detected by spectral domain optical coherence tomography in the optic nerve head and peripapillary retina in experimental glaucoma. Invest Ophthalmol Vis Sci. 2011b; 52:1206–1219. [PubMed: 21217108]

Strouthidis NG, Grimm J, Williams GA, Cull GA, Wilson DJ, Burgoyne CF. A Comparison of Optic Nerve Head Morphology Viewed by Spectral Domain Optical Coherence Tomography and By Serial Histology. Invest Ophthalmol Vis Sci. 2009

Strouthidis NG, White ET, Owen VM, Ho TA, Garway-Heath DF. Improving the repeatability of Heidelberg retina tomograph and Heidelberg retina tomograph II rim area measurements. Br J Ophthalmol. 2005a; 89:1433–1437. [PubMed: 16234447]

Strouthidis NG, White ET, Owen VM, Ho TA, Hammond CJ, Garway-Heath DF. Factors affecting the test-retest variability of Heidelberg retina tomograph and Heidelberg retina tomograph II measurements. Br J Ophthalmol. 2005b; 89:1427–1432. [PubMed: 16234446]

Sun D, Lye-Barthel M, Masland RH, Jakobs TC. The morphology and spatial arrangement of astrocytes in the optic nerve head of the mouse. J Comp Neurol. 2009; 516:1–19. [PubMed: 19562764]

Sun D, Qu J, Jakobs TC. Reversible reactivity by optic nerve astrocytes. Glia. 2013; 61:1218–1235. [PubMed: 23650091]

Takayama K, Hangai M, Kimura Y, Morooka S, Nukada M, Akagi T, Ikeda HO, Matsumoto A, Yoshimura N. Three-dimensional imaging of lamina cribrosa defects in glaucoma using swept-source optical coherence tomography. Invest Ophthalmol Vis Sci. 2013a; 54:4798–4807. [PubMed: 23778878]

Takayama K, Ooto S, Hangai M, Arakawa N, Oshima S, Shibata N, Hanebuchi M, Inoue T, Yoshimura N. High-resolution imaging of the retinal nerve fiber layer in normal eyes using adaptive optics scanning laser ophthalmoscopy. PLoS One. 2012; 7:e33158. [PubMed: 22427978]

Takayama K, Ooto S, Hangai M, Ueda-Arakawa N, Yoshida S, Akagi T, Ikeda HO, Nonaka A, Hanebuchi M, Inoue T, Yoshimura N. High-resolution imaging of retinal nerve fiber bundles in glaucoma using adaptive optics scanning laser ophthalmoscopy. Am J Ophthalmol. 2013b; 155:870–881. [PubMed: 23352341]

Tan O, Chopra V, Lu AT, Schuman JS, Ishikawa H, Wollstein G, Varma R, Huang D. Detection of macular ganglion cell loss in glaucoma by Fourier-domain optical coherence tomography. Ophthalmology. 2009; 116:2305–2314. e2301–2302. [PubMed: 19744726]

Tanna H, Dubis AM, Ayub N, Tait DM, Rha J, Stepien KE, Carroll J. Retinal imaging using commercial broadband optical coherence tomography. Br J Ophthalmol. 2010; 94:372–376. [PubMed: 19770161]

Tatham AJ, Miki A, Weinreb RN, Zangwill LM, Medeiros FA. Defects of the lamina cribrosa in eyes with localized retinal nerve fiber layer loss. Ophthalmology. 2014; 121:110–118. [PubMed: 24144452]

Tehrani S, Johnson EC, Cepurna WO, Morrison JC. Astrocyte processes label for filamentous actin and reorient early within the optic nerve head in a rat glaucoma model. Invest Ophthalmol Vis Sci. 2014; 55:6945–6952. [PubMed: 25257054]

Thanos S. The Relationship of Microglial Cells to Dying Neurons During Natural Neuronal Cell Death and Axotomy-induced Degeneration of the Rat Retina. Eur J Neurosci. 1991; 3:1189–1207. [PubMed: 12106219]

Thanos S, Indorf L, Naskar R. In vivo FM: using conventional fluorescence microscopy to monitor retinal neuronal death in vivo. Trends Neurosci. 2002; 25:441–444. [PubMed: 12183199]

Torti C, Povazay B, Hofer B, Unterhuber A, Carroll J, Ahnelt PK, Drexler W. Adaptive optics optical coherence tomography at 120,000 depth scans/s for non-invasive cellular phenotyping of the living human retina. Opt Express. 2009; 17:19382–19400. [PubMed: 19997159]

Townsend KA, Wollstein G, Schuman JS. Imaging of the retinal nerve fibre layer for glaucoma. Br J Ophthalmol. 2009; 93:139–143. [PubMed: 19028735]

Troutman TS, Barton JK, Romanowski M. Optical coherence tomography with plasmon resonant nanorods of gold. Opt Lett. 2007; 32:1438–1440. [PubMed: 17546147]

Tucker-Schwartz JM, Beavers KR, Sit WW, Shah AT, Duvall CL, Skala MC. In vivo imaging of nanoparticle delivery and tumor microvasculature with multimodal optical coherence tomography. Biomed Opt Express. 2014; 5:1731–1743. [PubMed: 24940536]

Tucker-Schwartz JM, Meyer TA, Patil CA, Duvall CL, Skala MC. In vivo photothermal optical coherence tomography of gold nanorod contrast agents. Biomed Opt Express. 2012; 3:2881–2895. [PubMed: 23162726]

Van Buskirk EM, Cioffi GA. Glaucomatous optic neuropathy. Am J Ophthalmol. 1992; 113:447–452. [PubMed: 1558122]

van der Schoot J, Vermeer KA, de Boer JF, Lemij HG. The effect of glaucoma on the optical attenuation coefficient of the retinal nerve fiber layer in spectral domain optical coherence tomography images. Invest Ophthalmol Vis Sci. 2012; 53:2424–2430. [PubMed: 22427540]

Vermeer KA, van der Schoot J, Lemij HG, de Boer JF. RPE-normalized RNFL attenuation coefficient maps derived from volumetric OCT imaging for glaucoma assessment. Invest Ophthalmol Vis Sci. 2012; 53:6102–6108. [PubMed: 22893674]

Vickers JC, Schumer RA, Podos SM, Wang RF, Riederer BM, Morrison JH. Differential vulnerability of neurochemically identified subpopulations of retinal neurons in a monkey model of glaucoma. Brain Res. 1995; 680:23–35. [PubMed: 7663981]

Vilupuru AS, Rangaswamy NV, Frishman LJ, Smith EL 3rd, Harwerth RS, Roorda A. Adaptive optics scanning laser ophthalmoscopy for in vivo imaging of lamina cribrosa. J Opt Soc Am A Opt Image Sci Vis. 2007; 24:1417–1425. [PubMed: 17429488]

Vizzeri G, Bowd C, Weinreb RN, Balasubramanian M, Medeiros FA, Sample PA, Zangwill LM. Determinants of agreement between the confocal scanning laser tomograph and standardized assessment of glaucomatous progression. Ophthalmology. 2010; 117:1953–1959. [PubMed: 20557941]

Vrabec F. Glaucomatous cupping of the human optic disk: a neuro-histologic study. Albrecht von Graefes Archiv fur klinische und experimentelle Ophthalmologie. Albrecht von Graefe's archive for clinical and experimental ophthalmology. 1976; 198:223–234. [PubMed: 1083166]

Walsh MK, Quigley HA. In vivo time-lapse fluorescence imaging of individual retinal ganglion cells in mice. J Neurosci Methods. 2008; 169:214–221. [PubMed: 18199485]

Wang B, Kagemann L, Schuman JS, Ishikawa H, Bilonick RA, Ling Y, Sigal IA, Nadler Z, Francis A, Sandrian MG, Wollstein G. Gold nanorods as a contrast agent for Doppler optical coherence tomography. PLoS One. 2014a; 9:e90690. [PubMed: 24595044]

Wang B, Nevins JE, Nadler Z, Wollstein G, Ishikawa H, Bilonick RA, Kagemann L, Sigal IA, Grulkowski I, Liu JJ, Kraus M, Lu CD, Hornegger J, Fujimoto JG, Schuman JS. In vivo lamina cribrosa micro-architecture in healthy and glaucomatous eyes as assessed by optical coherence tomography. Invest Ophthalmol Vis Sci. 2013; 54:8270–8274. [PubMed: 24302585]

Wang L, Burgoyne CF, Cull G, Thompson S, Fortune B. Static blood flow autoregulation in the optic nerve head in normal and experimental glaucoma. Invest Ophthalmol Vis Sci. 2014b; 55:873–880. [PubMed: 24436190]

Wang L, Cull G, Burgoyne CF, Thompson S, Fortune B. Longitudinal alterations in the dynamic autoregulation of optic nerve head blood flow revealed in experimental glaucoma. Invest Ophthalmol Vis Sci. 2014c; 55:3509–3516. [PubMed: 24812551]

Wang L, Dong J, Cull G, Fortune B, Cioffi GA. Varicosities of intraretinal ganglion cell axons in human and nonhuman primates. Invest Ophthalmol Vis Sci. 2003; 44:2–9. [PubMed: 12506048]

Wang M, Hood DC, Cho JS, Ghadiali Q, De Moraes CG, Zhang X, Ritch R, Liebmann JM. Measurement of local retinal ganglion cell layer thickness in patients with glaucoma using frequency-domain optical coherence tomography. Arch Ophthalmol. 2009; 127:875–881. [PubMed: 19597108]

Weber AJ, Kaufman PL, Hubbard WC. Morphology of single ganglion cells in the glaucomatous primate retina. Invest Ophthalmol Vis Sci. 1998; 39:2304–2320. [PubMed: 9804139]

Weinreb RN, Dreher AW, Coleman A, Quigley H, Shaw B, Reiter K. Histopathologic validation of Fourier-ellipsometry measurements of retinal nerve fiber layer thickness. Arch Ophthalmol. 1990; 108:557–560. [PubMed: 2322159]

Weinreb RN, Khaw PT. Primary open-angle glaucoma. Lancet. 2004; 363:1711–1720. [PubMed: 15158634]

Whitmore AV, Libby RT, John SW. Glaucoma: thinking in new ways-a role for autonomous axonal self-destruction and other compartmentalised processes? Prog Retin Eye Res. 2005; 24:639–662. [PubMed: 15953750]

Williams PA, Howell GR, Barbay JM, Braine CE, Sousa GL, John SW, Morgan JE. Retinal ganglion cell dendritic atrophy in DBA/2J glaucoma. PLoS One. 2013; 8:e72282. [PubMed: 23977271]

Wollstein G, Garway-Heath DF, Fontana L, Hitchings RA. Identifying early glaucomatous changes. Comparison between expert clinical assessment of optic disc photographs and confocal scanning ophthalmoscopy. Ophthalmology. 2000; 107:2272–2277. [PubMed: 11097609]

Wollstein G, Paunescu LA, Ko TH, Fujimoto JG, Kowalevicz A, Hartl I, Beaton S, Ishikawa H, Mattox C, Singh O, Duker J, Drexler W, Schuman JS. Ultrahigh-resolution optical coherence tomography in glaucoma. Ophthalmology. 2005a; 112:229–237. [PubMed: 15691556]

Wollstein G, Schuman JS, Price LL, Aydin A, Stark PC, Hertzmark E, Lai E, Ishikawa H, Mattox C, Fujimoto JG, Paunescu LA. Optical coherence tomography longitudinal evaluation of retinal nerve fiber layer thickness in glaucoma. Arch Ophthalmol. 2005b; 123:464–470. [PubMed: 15824218]

Yamanari M, Lim Y, Makita S, Yasuno Y. Visualization of phase retardation of deep posterior eye by polarization-sensitive swept-source optical coherence tomography with 1-microm probe. Opt Express. 2009; 17:12385–12396. [PubMed: 19654640]

Yang H, He L, Gardiner SK, Reynaud J, Williams G, Hardin C, Strouthidis NG, Downs JC, Fortune B, Burgoyne CF. Age-related differences in longitudinal structural change by spectral-domain optical coherence tomography in early experimental glaucoma. Invest Ophthalmol Vis Sci. 2014; 55:6409–6420. [PubMed: 25190652]

Yang H, Qi J, Hardin C, Gardiner SK, Strouthidis NG, Fortune B, Burgoyne CF. Spectral-domain optical coherence tomography enhanced depth imaging of the normal and glaucomatous nonhuman primate optic nerve head. Invest Ophthalmol Vis Sci. 2012a; 53:394–405. [PubMed: 22159003]

Yang Q, Cho KS, Chen H, Yu D, Wang WH, Luo G, Pang IH, Guo W, Chen DF. Microbead-induced ocular hypertensive mouse model for screening and testing of aqueous production suppressants for glaucoma. Invest Ophthalmol Vis Sci. 2012b; 53:3733–3741. [PubMed: 22599582]

Yin L, Geng Y, Osakada F, Sharma R, Cetin AH, Callaway EM, Williams DR, Merigan WH. Imaging light responses of retinal ganglion cells in the living mouse eye. J Neurophysiol. 2013; 109:2415–2421. [PubMed: 23407356]

Yin L, Masella B, Dalkara D, Zhang J, Flannery JG, Schaffer DV, Williams DR, Merigan WH. Imaging light responses of foveal ganglion cells in the living macaque eye. J Neurosci. 2014; 34:6596–6605. [PubMed: 24806684]

Yoshikawa M, Akagi T, Hangai M, Ohashi-Ikeda H, Takayama K, Morooka S, Kimura Y, Nakano N, Yoshimura N. Alterations in the neural and connective tissue components of glaucomatous

cupping after glaucoma surgery using swept-source optical coherence tomography. Invest Ophthalmol Vis Sci. 2014; 55:477–484. [PubMed: 24398100]

You JY, Park SC, Su D, Teng CC, Liebmann JM, Ritch R. Focal lamina cribrosa defects associated with glaucomatous rim thinning and acquired pits. JAMA ophthalmology. 2013; 131:314–320. [PubMed: 23370812]

Yucel YH, Gupta N, Kalichman MW, Mizisin AP, Hare W, de Souza Lima M, Zangwill L, Weinreb RN. Relationship of optic disc topography to optic nerve fiber number in glaucoma. Arch Ophthalmol. 1998; 116:493–497. [PubMed: 9565048]

Zangwill LM, Bowd C. Retinal nerve fiber layer analysis in the diagnosis of glaucoma. Curr Opin Ophthalmol. 2006; 17:120–131. [PubMed: 16552246]

Zangwill LM, Jain S, Dirkes K, He F, Medeiros FA, Trick GL, Brandt JD, Cioffi GA, Coleman AL, Liebmann JM, Piltz-Seymour JR, Gordon MO, Kass MA, Weinreb RN. The rate of structural change: the confocal scanning laser ophthalmoscopy ancillary study to the ocular hypertension treatment study. Am J Ophthalmol. 2013; 155:971–982. [PubMed: 23497845]

Zangwill LM, Weinreb RN, Beiser JA, Berry CC, Cioffi GA, Coleman AL, Trick G, Liebmann JM, Brandt JD, Piltz-Seymour JR, Dirkes KA, Vega S, Kass MA, Gordon MO. Baseline topographic optic disc measurements are associated with the development of primary open-angle glaucoma: the Confocal Scanning Laser Ophthalmoscopy Ancillary Study to the Ocular Hypertension Treatment Study. Arch Ophthalmol. 2005; 123:1188–1197. [PubMed: 16157798]

Zawadzki RJ, Choi SS, Fuller AR, Evans JW, Hamann B, Werner JS. Cellular resolution volumetric in vivo retinal imaging with adaptive optics-optical coherence tomography. Opt Express. 2009; 17:4084–4094. [PubMed: 19259248]

Zawadzki RJ, Jones SM, Olivier SS, Zhao M, Bower BA, Izatt JA, Choi S, Laut S, Werner JS. Adaptive-optics optical coherence tomography for high-resolution and high-speed 3D retinal in vivo imaging. Opt Express. 2005; 13:8532–8546. [PubMed: 19096728]

Zawadzki RJ, Jones SM, Pilli S, Balderas-Mata S, Kim DY, Olivier SS, Werner JS. Integrated adaptive optics optical coherence tomography and adaptive optics scanning laser ophthalmoscope system for simultaneous cellular resolution in vivo retinal imaging. Biomed Opt Express. 2011; 2:1674–1686. [PubMed: 21698028]

Zeimer R, Asrani S, Zou S, Quigley H, Jampel H. Quantitative detection of glaucomatous damage at the posterior pole by retinal thickness mapping. A pilot study. Ophthalmology. 1998; 105:224–231. [PubMed: 9479279]

Zhang X, Hu J, Knighton RW, Huang XR, Puliafito CA, Jiao S. Dual-band spectral-domain optical coherence tomography for in vivo imaging the spectral contrasts of the retinal nerve fiber layer. Opt Express. 2011; 19:19653–19659. [PubMed: 21996906]

Zhang Y, Rha J, Jonnal R, Miller D. Adaptive optics parallel spectral domain optical coherence tomography for imaging the living retina. Opt Express. 2005; 13:4792–4811. [PubMed: 19495398]

Zhi Z, Cepurna W, Johnson E, Shen T, Morrison J, Wang RK. Volumetric and quantitative imaging of retinal blood flow in rats with optical microangiography. Biomed Opt Express. 2011; 2:579–591. [PubMed: 21412463]

Zhi Z, Cepurna WO, Johnson EC, Morrison JC, Wang RK. Impact of intraocular pressure on changes of blood flow in the retina, choroid, and optic nerve head in rats investigated by optical microangiography. Biomed Opt Express. 2012; 3:2220–2233. [PubMed: 23024915]

Zhou Q, Knighton RW. Light scattering and form birefringence of parallel cylindrical arrays that represent cellular organelles of the retinal nerve fiber layer. Applied Optics. 1997; 36:2273–2285. [PubMed: 18253203]

Zotter S, Pircher M, Gotzinger E, Torzicky T, Yoshida H, Hirose F, Holzer S, Kroisamer J, Vass C, Schmidt-Erfurth U, Hitzenberger CK. Measuring retinal nerve fiber layer birefringence, retardation, and thickness using wide-field, high-speed polarization sensitive spectral domain OCT. Invest Ophthalmol Vis Sci. 2013; 54:72–84. [PubMed: 23221076]

The most common techniques in current use for in vivo assessment of ocular structure in animal models of experimental glaucoma include optical coherence tomography and scanning laser ophthalmoscopy.

These and other imaging modalities can be used in clinical studies as well as in laboratory animal studies of glaucoma models to quantify structural parameters of the optic nerve head, retinal nerve fiber layer, retinal ganglion cell soma and dendrites.

Incorporating in vivo imaging into laboratory studies, the glaucoma research community can not only reduce the number of animals needed to achieve robust outcomes, but also refine and prove relevance of EG models to hasten the translation of discovery from bench-to-bedside.

Recent developments hold extraordinary promise for revealing important events in glaucoma pathogenesis in living eyes as well as for identification of specific cellular and molecular targets for imaging in vivo.

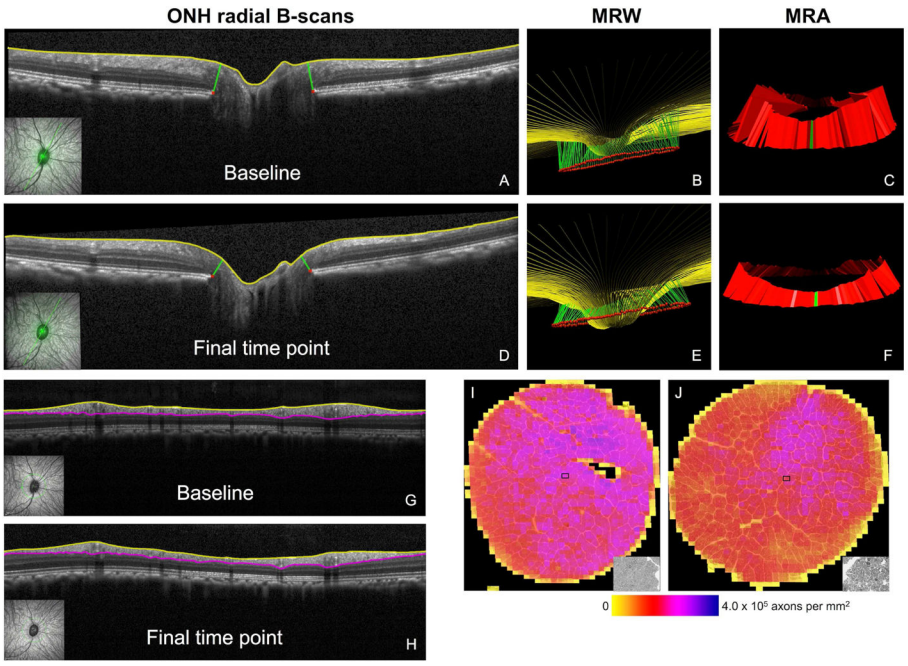

Figure 1. ONH parameters obtained from SDOCT radial scans under manometric IOP control

Individual example of an NHP EG eye imaged at its first baseline (**A, B, C**) and at its final time point (**D, E, F**) just prior to sacrifice. Insets in the lower left corner of A and D show the location of the B-scan as indicated by the bold green line overlaid onto the infrared CSLO reflectance image. Structures delineated in each radial B-scan include the ILM (yellow) and BMO points (red). The green segments connecting BMO points to the ILM represent the pair of MRW measurements made in each radial B-scan. Results for all 80 B-scans are shown projected from 3D for the baseline (B) and final time point (E). Note deformation of the ONH apparent in E, including a deeper "cup" and thinner "rim". Global average MRW decreased from 330 μm at baseline to 200 μm at the final time point (−40%). MRA decreased from 1.11 mm^2 at baseline (C) to 0.69 mm^2 at the final time point (F, **−38%**). Segmentation of peripapillary circular B-scans to obtain the parameter RNFL thickness are shown for the same eye and time points in **G** and **H**. Segmentations are shown for the ILM (yellow) and posterior RNFL boundary (magenta). Global average RNFL thickness decreased from 107.1 μm at baseline (G) to 82.9 μm at the final time point (H, −23%). Optic nerve axon counts for both eyes (the EG eye and fellow control eye) of the same animal (**I,J**). All axons were counted from 100% of the cross-sectional area of each optic nerve. Shown here are the composited montages of all image tiles used to count axons for the control eye (**I**) and EG eye (**J**) of the same NHP shown in panels A–H. Axon density of each tile is color-coded, insets show a magnified view of a single tile. Total axon count was 1,319,268 in the control eye and 1,001,512 in the EG eye (−24.1%). As reported by Hardin *et al.* (IOVS 2015;56:ARVO E-Abstract 1010) and Fortune *et al.* (IOVS 2015;56:ARVO E-Abstract 3982), the ONH parameters MRW and MRA are "more sensitive" than RNFL thickness insofar as they discriminate better between EG and control eyes and change at an earlier stage of damage (less axon loss), but peripapillary RNFL thickness is more strongly correlated with axon loss than MRW or MRA. Both observations

are most likely caused by ONH connective tissue deformations contributing more to ONH rim thinning than to peripapillary RNFL thickness changes, whereas axon loss dominates the change in peripapillary RNFL thickness.

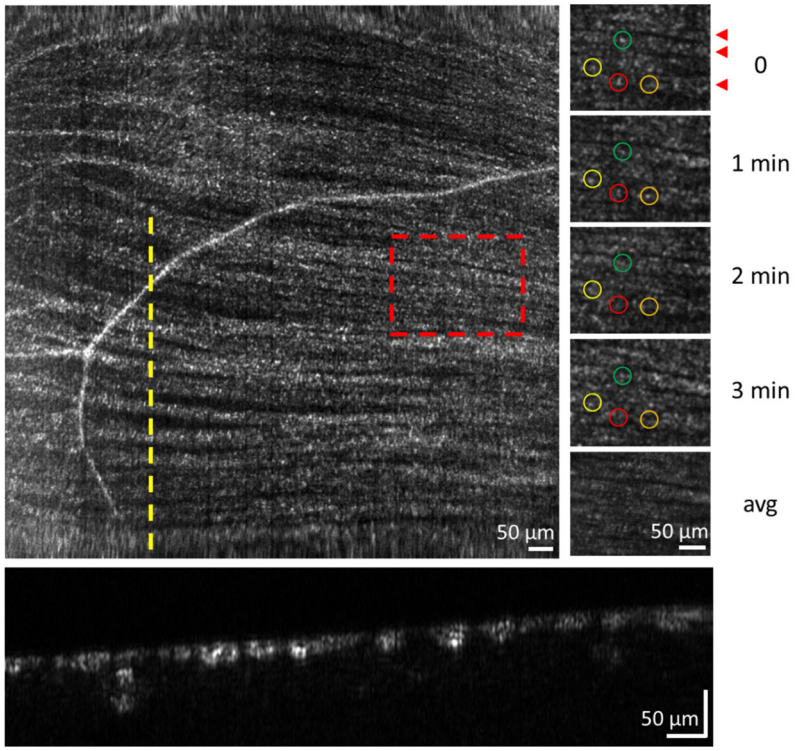

Figure 2.

Imaging axonal activity in a human eye. (Left) MHz AO-OCT *en face* projection of RNFL bundles centered 3.5° nasal to the fovea. I mage is from a single volume acquired at a rate of 1 million A-lines/s (1 MHz), covering 3.6°x3.6° with 1 µm/pixel lateral sampling.(Kocaoglu et al., 2014b) (Right) Time sequence of a subsection of RNFL bundles from the red dashed region of the left image. Colored labels denote bundle locations at which reflectance was measured every minute over a 3 minute period. Bottom image of column is an average of the four time points. Red arrowheads at t=0 point to individual RNFL bundles. (Bottom) Cross section of RNFL bundles extracted at the location of the yellow dashed line in the left image. Figure courtesy of Zhuolin Liu, Omer Kocaoglu and Don Miller, Indiana University.

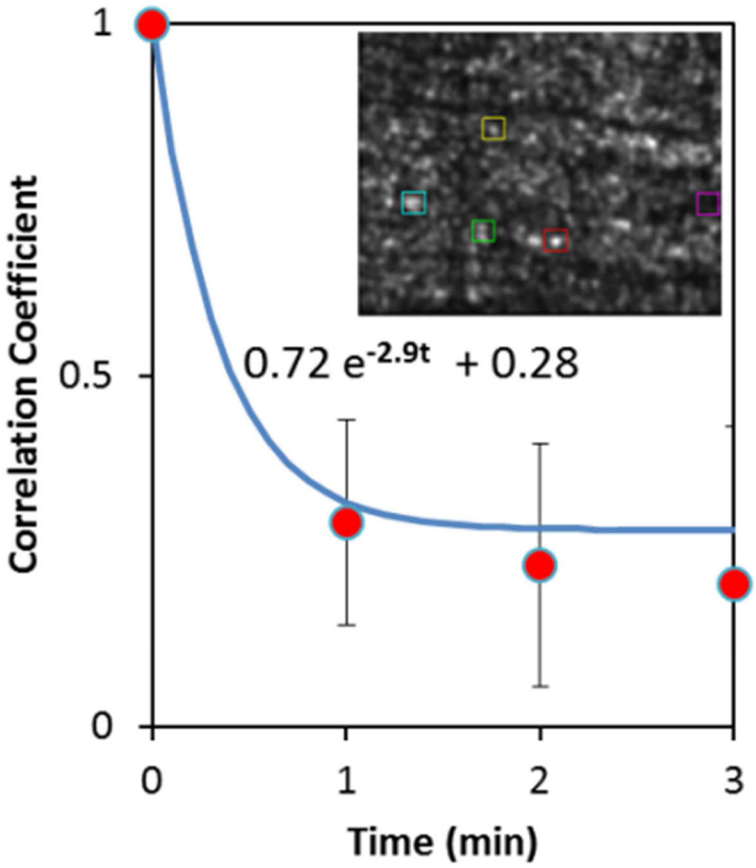

Figure 3.

Measurement of axonal activity. Correlation coefficient *vs.* time for RNFL bundle scatter dynamics of the labeled squares in the RNFL bundle image (inset and in Fig. 1). Exponential decay with 0.34 min time constant (blue curve) is consistent with results reported by Huang et al.(Huang et al., 2013) for *in vitro* rat retina. Figure courtesy of Zhuolin Liu, Omer Kocaoglu and Don Miller, Indiana University.

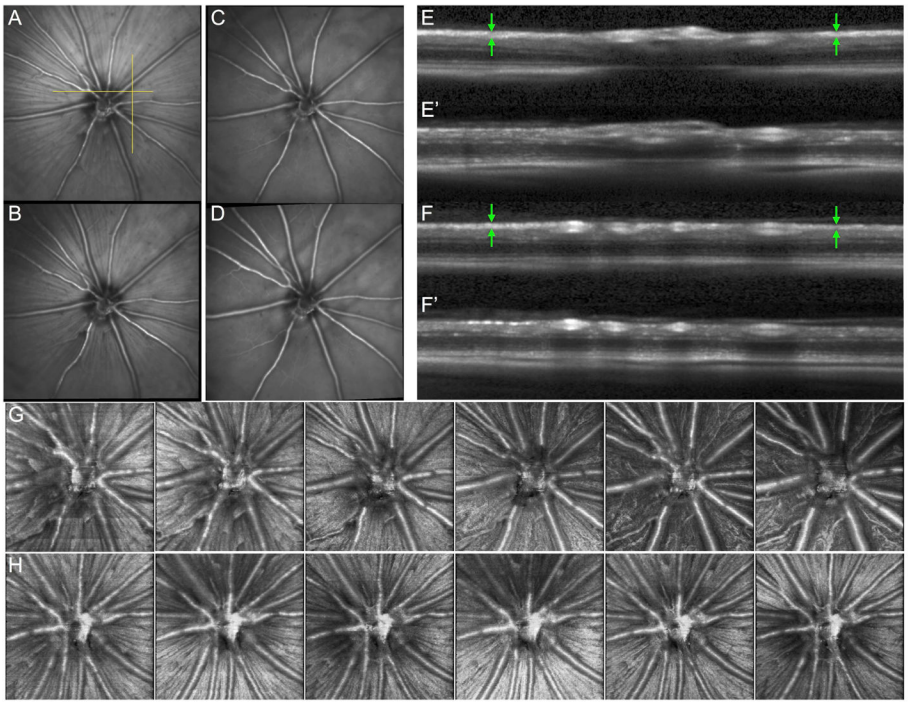

Figure 4.

Example of longitudinal imaging by CSLO and SDOCT (Spectralis HRA+OCT, Heidelberg Engineering, GmbH) in a pigmented rat during baseline and four weekly follow-ups after unilateral optic nerve transection.(Choe et al., 2014) (**A**) Infrared reflectance image obtained by CSLO (30 x 30 deg) at one baseline time point; (**B**) follow-up time point 1 week after transection; (**C**) 3 weeks after transection; (**D**) 4 weeks after transection. RNFL bundle reflectance has nearly completely disappeared by 4-weeks while the contrast of the major retinal vessels and capillaries has become more prominent against the fundus background. SDOCT volumes consisting of 290 horizontal B-scans (15 x 15 deg) were obtained weekly during baseline and at each of the 4 follow-ups. (**E**) An example B-scan from the position indicated by the horizontal yellow line in A. (**F**) An interpolated slice through the SDOCT volume at the position shown by the vertical yellow line in A. The healthy RNFL at baseline (E and F, green arrows) is nearly completely thinned 4 weeks after transection E' and F'. (**G and H**) En face projections from the SDOCT volumes across the entire longitudinal series are shown for the transected eye in row G and the fellow control eye in row H. The RNFL progressively disappears over weeks 2–4 in the transected eye. Each panel shows the sum voxel projection for a 10-pixel slab beginning at the internal limiting membrane (e.g. downward arrows in E and F).

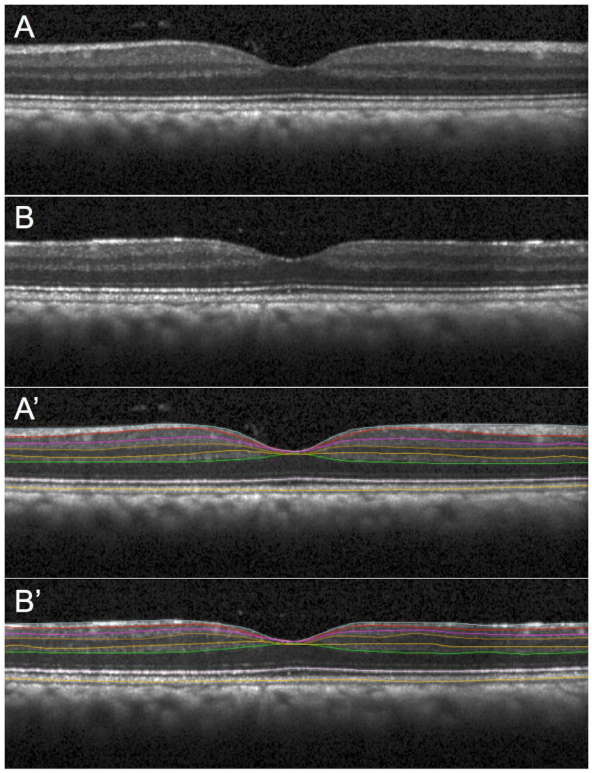

Figure 5. Macular retinal layer thickness parameters obtained from SDOCT radial scans under manometric IOP control

Individual example of an NHP EG eye imaged at baseline (**A, A'**) and at its final time point (**B, B'**) just prior to sacrifice when glaucomatous damage was severe (as determined by complete orbital optic nerve axon counts). One of 48 B-scans (vertical orientation) from a radial pattern centered on the fovea is shown without segmentation in A and B, with layer segmentations in A' and B'. This example is representative of the pattern of results observed across N=21 NHP in this study: there was clear, consistent loss in EG eyes of macular nerve fiber layer, ganglion cell layer and inner plexiform layer thickness, along with a small but significant increase in this thickness of both the outer plexiform layer and a layer defined as the outer nuclear (photoreceptor cell) layer plus inner segments and Henle's fibers, with no change in outer segment length (defined as being from the reflectivity band at the inner segment-outer segment junction to the band at the cone outer segment tips, "COST line"). Macular inner retinal layer thickness losses were strongly correlated with peripapillary RNFL thickness in EG eyes but the subtle increase of outer retinal layer thickness was only weakly correlated with loss peripapillary RNFL thickness. Macular inner retinal layer losses were correlated with loss of function specific to retinal ganglion cells derived from multifocal electroretinography, while function of distal retinal elements was unchanged relative to fellow control eyes and un-related to peripapillary RNFL thickness loss. From Wilsey et al., *Invest Ophthalmol Vis Sci* 2015;56: E-Abstract 638.